National Renewable Energy Laboratory
A national laboratory of the U.S. Department of Energy
Office of Energy Efficiency & Renewable Energy
Innovation for Our Energy Future

Innovative Characterization of Amorphous and Thin-Film Silicon for Improved Module Performance

1 February 2005 – 31 July 2008

P.C. Taylor and G.A. Williams
University of Utah
Salt Lake City, Utah

Subcontract Report
NREL/SR-520-46649
September 2009

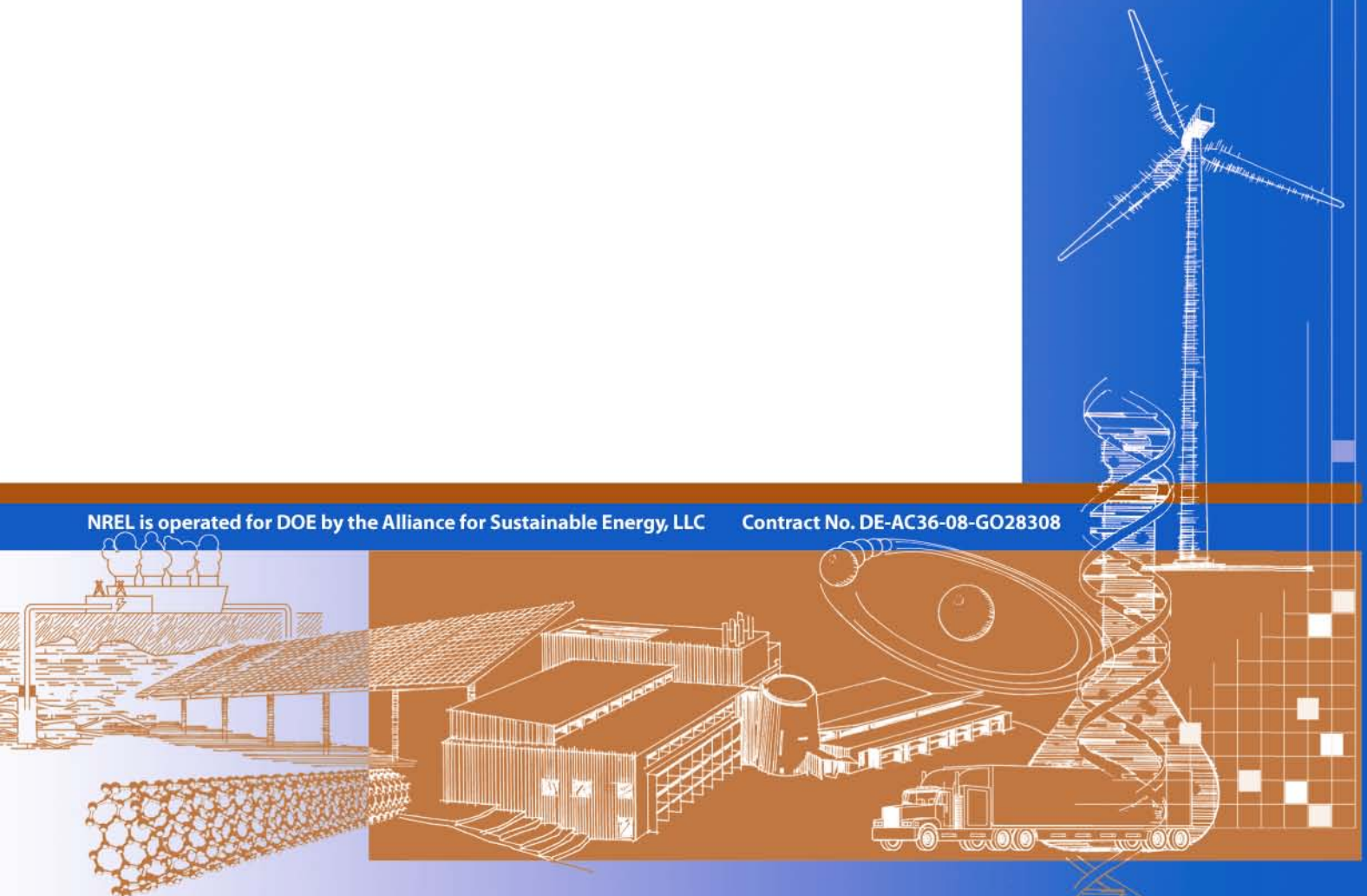

NREL is operated for DOE by the Alliance for Sustainable Energy, LLC Contract No. DE-AC36-08-GO28308

Innovative Characterization of Amorphous and Thin-Film Silicon for Improved Module Performance

1 February 2005 – 31 July 2008

P.C. Taylor and G.A. Williams
University of Utah
Salt Lake City, Utah

NREL Technical Monitor: Name: Bolko von Roedern

Prepared under Subcontract No. XXL-5-44205-09

Subcontract Report
NREL/SR-520-46649
September 2009

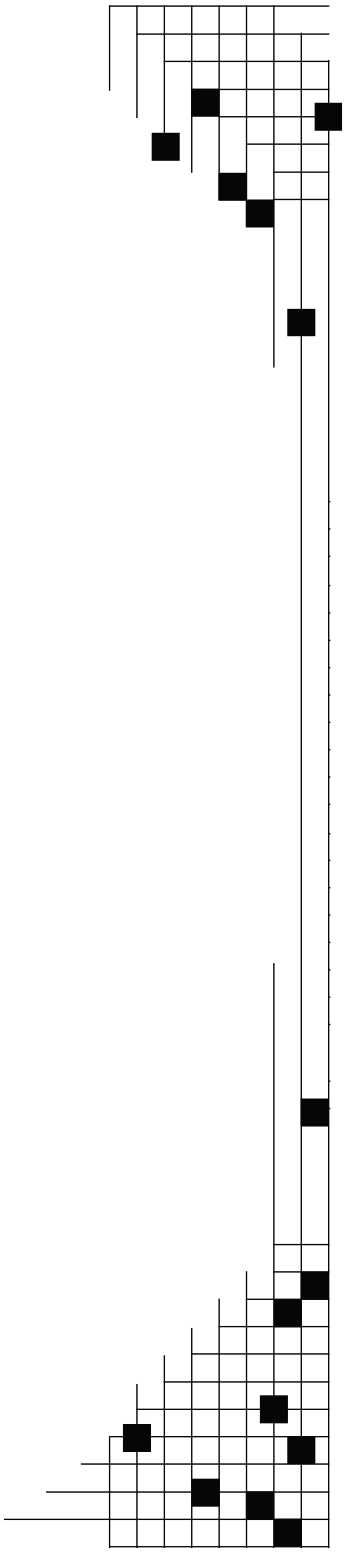

National Renewable Energy Laboratory
1617 Cole Boulevard, Golden, Colorado 80401-3393
303-275-3000 • www.nrel.gov

NREL is a national laboratory of the U.S. Department of Energy
Office of Energy Efficiency and Renewable Energy
Operated by the Alliance for Sustainable Energy, LLC

Contract No. DE-AC36-08-GO28308

Table of Contents

I. Introduction

Research results during the duration of NREL Subcontract XXL-5-44205-09 are reported. We performed collaborative research with United Solar Ovonics Corporation on defects that contribute to the Staebler-Wronski effect in modules made using a-Si:H and a-Si_xGe_{1-x}:H intrinsic layers. Specifically, we performed electron spin resonance (ESR) on a set of device-quality samples, half of which were light soaked. We also performed nuclear magnetic resonance (NMR) experiments on these samples to investigate hydrogen doublet sites. In addition, we investigated the defects generated in tritiated a-Si:H at both 300 and 77 K in collaboration with scientists at NREL. Finally, we performed studies of light soaking at 77 K to compare the kinetics with those for the creation of defects at 77 K by tritium decay.

II. The Hydrogen Doublet Defect

We have previously reported an ^{1}H NMR signal in a-Si:H that occurs only after light soaking for 600 hours [1]. This signal, which is attributed to a pair of hydrogen atoms, exhibits similar annealing kinetics to that of the defects created during light-soaking, and the concentration of these sites is comparable to that of the defects measured by electron spin resonance (ESR). The distance between the two hydrogen atoms in the pair is about 2.3 Å. Preliminary data on the temperature dependence of the lineshape suggested that the pair may undergo some form of local motion as the temperature increases [1], but the evidence was not compelling. In addition, our earlier measurements could not exclude the possibility that the additional lineshape was due to a hydrogen triplet with the central peak masked by the narrow line from bonded hydrogen. We have recently investigated the lineshape of this ^{1}H NMR feature in further detail as well as its temperature dependence at a magnetic field, B_0, of 3.5 T.

We have found that the spin-lattice relaxation time (T_1) of the doublet has a strong temperature dependence, which may indicate a thermally activated motion. However, this dependence cannot be explained by a simple thermally activated, random diffusive process, such as that described by the Bloembergen, Purcell, and Pound model (BPP model). In particular, for temperatures between 6.5 and 20 K we find no evidence that the doublet lineshape is narrowed due to motional effects as would be expected if the simplest BPP model applied.

These experiments were performed on a light-soaked, thin film of *a*-Si:H, which was originally made at BP Solar in a large area deposition system by DC plasma enhanced chemical vapor deposition (PECVD). The film was light-soaked for 600 hr with a solar simulator. We have published the details of the sample preparation elsewhere [1,2]. Details of the NMR measurements can also be found elsewhere [1]. We have used our standard technique to suppress the much stronger signal from hydrogen bonded to silicon atoms, namely, a Jeener-Broekaert three-pulse sequence [3]. The NMR line shapes are obtained by recording the stimulated echo after the Jeener-Broekaert sequence. The echo intensity $I(\tau_1, \tau_2)$ is given by [4]

$$I(\tau_1,\tau_2) = I_0 \exp\{-\frac{2\tau_1}{T_2}\} \exp\{-(\frac{\tau_2}{T_{1D}})^{\frac{1}{2}}\} \quad , \tag{1}$$

where τ_1 and τ_2 are the separations between the first and second pulses, and the second and third pulses, respectively. T_2 and T_{1D} are the spin-spin relaxation time and the dipolar spin lattice relaxation time, respectively. A typical pulse width for the 90° pulse is about 2 μs.

At a ^{1}H NMR frequency ω_0 = 147.417 MHz and at low temperatures, the values of T_1 for the hydrogen, which is bonded to silicon (bonded hydrogen), are too long for these hydrogen sites to fully recover using a practical pulse repetition rate. Therefore the signal from the bonded hydrogen is suppressed due to partial saturation. The dependence of the NMR signal I on the delay time between two scans, T_d, is,

$$I = I_0(1 - e^{-T_d/T_1}), \tag{2}$$

where I_0 is the amplitude of the fully relaxed signal. The inverse of T_d is the rate at which the three-pulse sequence is repeated (repetition rate). When $T_d << T_1$, the relation becomes,

$$I = I_0 \frac{T_d}{T_1} . \tag{3}$$

Figure 1 shows the temperature dependence of the NMR line shapes at B_0 = 3.5 T. The lineshape obtained earlier [1] at B_0 = 2 T and T = 7 K is also shown for comparison. [In all line shapes shown in this report the Zeeman frequency has been subtracted so that the peaks are centered about zero.] The composite line shapes contain a narrow line (~ 4 kHz FWHM) and a broad line (~ 25 kHz FWHM) as is always seen in typical a-Si:H samples prepared by the PECVD technique. The narrow line is attributed to randomly occurring hydrogen atoms that are bonded to silicon, hereafter termed "dilute" hydrogen. The broad line is attributed to hydrogen atoms bonded to silicon in a clustered configuration, hereafter termed "clustered" hydrogen. In addition, a small doublet occurs with a splitting $\Delta\nu$ = 15 kHz as indicated by the dashed lines. As can be seen from Fig. 1, $\Delta\nu$ is constant for B_0 = 2 T and B_0 = 3.5 T. At B_0 = 3.5 T, $\Delta\nu$ remains the same, within the experimental error, at T = 7 K and T = 10 K. The doublet is less obvious at T = 6.5 T and T = 20 K. As we will discuss below, this behavior is attributed to the different temperature dependences of the T_1's for the bonded hydrogen and the doublet. A detailed comparison of the composite lineshape shows that no motional narrowing of the doublet occurs for temperatures up to 20 K.

Figure 2 shows the temperature dependence of T_1 for both the bonded hydrogen and the doublet, plotted as log(T_1) against 1000/T. Open circles denote the data for bonded hydrogen. Solid circles denote the data for the doublet. The lines are aids to the eye. The value of T_1 for bonded hydrogen, hereafter denoted as $T_1(B)$, at 4.2 K is an extrapolation from the data at 92.5 MHz [3], assuming a field dependence of T_1 as $T_1 \propto \varpi^2$. As can be seen in Fig. 2, T_1 of the doublet, hereafter denoted as $T_1(D)$, increases much more rapidly than $T_1(B)$, as the temperature decreases. For temperatures below about 6 K, $T_1(D) > T_1(B)$. This relationship means that at the

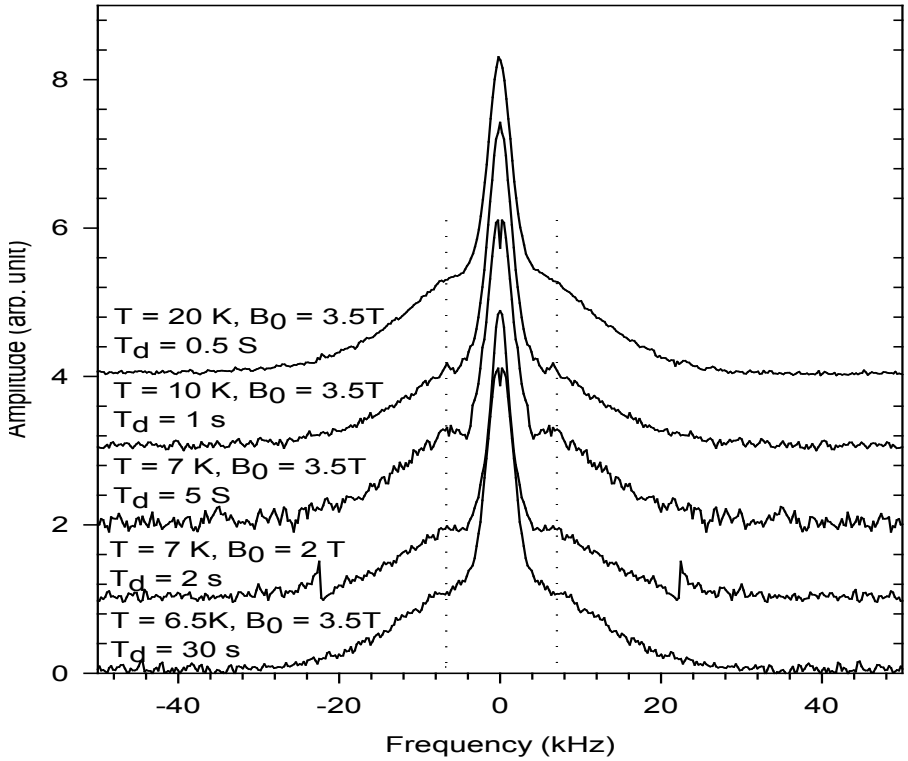

Figure 1. ^{1}H NMR line shapes from the light-soaked sample at different temperatures and at two magnetic fields, B_0 = 2 T and B_0 = 3.5 T. The two dashed lines indicate where the doublet appears.

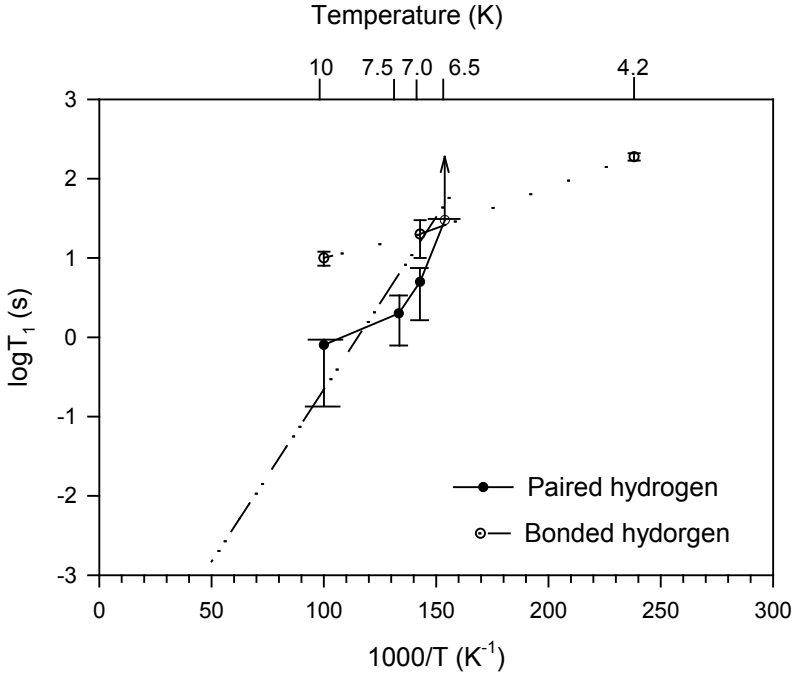

Figure 2. Temperature dependence of T_1 for the hydrogen doublet and the bonded hydrogen. The open circles represent the data for bonded hydrogen. The solid circles represent the data for the hydrogen doublet. The lines are aids to the eye. The dashed-dotted line is a straight line with a slope of 100 K. See text for details.

lowest temperatures the signal from the bonded hydrogen will recover faster than that of the doublet, resulting in an apparent suppression of the signal from the doublet. On the other hand, at $T = 20$ K, $T_1(B)$ is short enough compared to the pulse repetition rate so that most of the signal from bonded hydrogen fully recovers, and once again effectively reduces the signal from the doublet. In short, the doublet only becomes visible when the signal from bonded hydrogen is drastically reduced by the dipolar echo sequence (due to a much more rapid T_{1d}) and also reduced by partial saturation (due to a much longer T_1).

Figure 3 shows the comparison of the lineshape at 7 K, with a recovery time $T_d = 5$ s, and the lineshape at 20 K with $T_d = 0.5$ s, in which the signal from the bonded hydrogen has relaxed and the signal from the doublet is effectively suppressed. Solid circles and open circles represent the data at 7 K and 20 K, respectively. The solid line represents a subtraction of the 20 K data from the 7 K data, and the dashed line is a fit to this subtraction with a Pake doublet powder pattern that is broadened isotropically by a Gaussian whose width is approximately 10% of the splitting between the two divergences. The sharp negative spike near the center is an artifact due to small phase errors in the complex Fourier transforms. The splitting between the two divergences is about 16 kHz. This value is consistent with that previously estimated from measurements at a lower frequency [1].

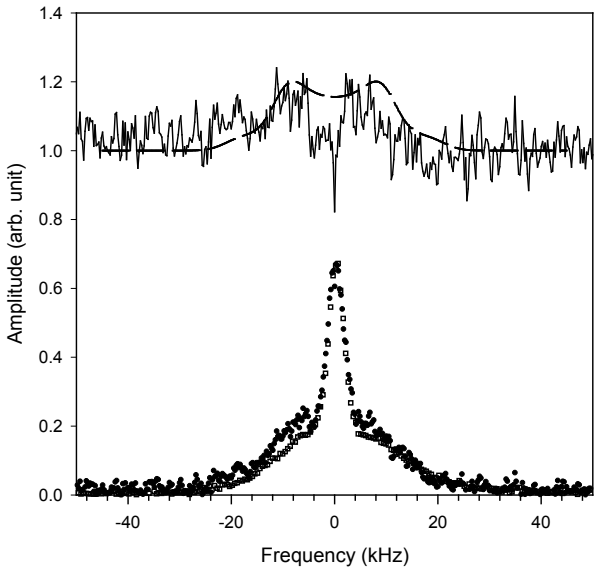

Figure 3. ^{1}H NMR line shapes from the light-soaked sample at different temperatures and at a magnetic field $B_0 = 3.5$ T. Solid circles represent data at 7 K taken with $T_d = 5$ s. Open circles represent data at 20 K taken with $T_d = 0.5$ s. The solid line represents the difference between the data at 7 K and 10 K. The dashed line is a fit using a Pake doublet powder pattern broadened isotropically by about 2 kHz, with a splitting between the two divergences of 16 kHz. See text for details.

The most interesting result of this study is the strong temperature dependence of the spin-lattice relaxation time of the doublet. In particular, for temperatures between 6.5 K and 20 K, the values of T_1 for the doublet are shorter than those of the bonded hydrogen. Since most of the intensity in the doublet line is well outside the width of the narrow line, the dipole-dipole coupling between the doublet and the dilute hydrogen should be rather weak. Therefore, if the

relaxation mechanism were the same (spin diffusion of the energy to a molecular hydrogen relaxation center) the T_1 for the doublet should, if anything, be longer than that of the bonded hydrogen. Since the T_1 of the doublet is actually shorter, there must be a different relaxation mechanism. Specifically, there must be a relaxation center close to the hydrogen doublet that is more efficient than spin diffusion to molecular hydrogen. A paramagnetic "impurity", such as a silicon dangling bond, is one possibility, but in this case one must explain why this paramagnetic center does not also shorten the T_{1d} of the doublet and why the doublets occur preferentially near such a relaxation center.

A second possibility is thermally activated local motion of the hydrogen pairs. The simplest case is the BPP-type relaxation, in which the atoms jump randomly between different sites due to thermal activation. The local dipolar field experienced by the nuclei is modulated, and therefore induces relaxation of the nuclei. If one assumes a thermally activated hopping of hydrogen atoms, the hopping time τ can be expressed as

$$\tau^{-1} = \tau_0^{-1} e^{-E_a / kT}, \qquad (4)$$

where E_a is the activation energy and τ_0 is a pre-factor that is, on the order of a phonon frequency.

In the BPP model T_1 is given as

$$T_1 \propto \left(\frac{\omega_0}{\Delta\omega} \right)^2 \tau_0 e^{E_a / kT}, \qquad (5)$$

where $\Delta\omega$ is on the order of the dipolar line width and ω_0 is the Zeeman frequency. In our case, eq. 5 does not appear to hold because the dependence of T_1 on ω_0 is weaker than quadratic. In addition, for reasonable choices of $\Delta\omega$ and τ_0 the observed values of T_1 imply that the doublet lineshape should be motionally narrowed, which is also not the case. Earlier works have suggested that if there exists a distribution of τ, which is very likely in disordered materials, then one might be able to fit the observed temperature dependence of T_1 consistently [5,6]; however, even if this is the case, the observed lineshape will be a sum of the line shapes with hydrogen atoms at different sites, and one would again expect a change in lineshape with temperature. Therefore, if the hydrogen pairs are undergoing local motion, it must be some form of correlated motion that maintains the distance between the two hydrogen atoms in a pair.

The second issue is the absence of motional narrowing of the doublet lineshape. From T = 6.5 K up to T = 20 K, the doublet lineshape remains unchanged. In the case of the random hopping of the atoms, motional narrowing of the NMR line occurs when $\tau = (\Delta\nu)^{-1}$, where $\Delta\nu$ is the line width. For the doublet, $\Delta\nu$ = 16 kHz, which gives a value of τ between 10^{-5} and 10^{-4} s. Our calculation shows that the temperature at which the narrowing should occur is below 6 K, but we observe no narrowing between 6.5 K and 20 K. The microscopic mechanism for the spin lattice relaxation of the hydrogen doublet is currently unknown.

In summary, we have investigated the temperature dependence of the paired hydrogen site that is associated with light-soaking. We find that the spin-lattice relaxation time of these paired hydrogen atoms strongly depends on temperature between 6.5 K and 20 K. A simple model assuming that hydrogen atoms are hopping randomly between different sites cannot explain this dependence. For temperatures between 6.5 K and 20 K, we do not observe motional narrowing. A subtraction of the spectra at 7 K and 20 K provides an approximate lineshape for the site associated with light soaking and supports the attribution of this site to a pair of hydrogen atoms, which are approximately 2.3 Å apart.

III. Silicon Dihydride and Silicon Doublets

a. Silicon Dihydride Bonding

Since the discovery of the Staebler-Wronski effect (SWE), many studies have contributed to our understanding of the role of hydrogen in producing this metastable effect in hydrogenated amorphous silicon (a-Si:H). Models of this metastability, such as those of Stutzmann et al. [7] and Branz [8], have the common component that hydrogen must play a role in forming or stabilizing a metastable site [7,8]. Our recent ^{1}H NMR studies of device quality *a-Si:H* have found a paired hydrogen site (*H-H*) with an *H-H* distance of 2.3 ± 0.2 Å [9]. This previous study indicates that the *H-H* site is probably metastable; however, the study does not identify the specific *H-H* bonding configuration. A natural candidate for the bonding configuration is SiH_2, which is predicted to have an *H-H* separation of 2.4 Å, assuming a tetrahedral structure with a *Si-H* bond length of 1.5 Å. Furthermore, a recent calculation by Tasfaye *et al.* demonstrates the existence of SiH_2 in the amorphous network with an *H-H* separation of approximately 2.4 Å [10]. Although these results are suggestive, no conclusive measurements of the *H-H* distance for SiH_2 have been performed in the *a-Si:H* system.

The difficulty with assuming that SiH_2 is the metastable site derives from a stability argument. Annealing studies have shown little change in SiH_2 concentrations for temperatures up to 600 K [11], and yet it is known that annealing of metastable defects occurs at temperatures of ~ 200° C. From these disparate temperature dependences it seems unlikely that SiH_2 is created or destroyed during light soaking and subsequent annealing. It is possible that the metastable doublet observed by Su *et al.* somehow becomes observable in the NMR experiments after light soaking, but there are some compelling arguments to suggest that this is not the case [9].

These considerations have motivated the current work. In particular, by combining NMR and far infrared spectroscopic evidence, we have positively identified a specific NMR lineshape as due to SiH_2 and presented the first detailed ^{1}H NMR study of stable SiH_2 in *a-Si:H*.

The sample used for this set of experiments was grown at United Solar Ovonics using plasma enhanced chemical vapor deposition (PECVD) of silane (SiH_4). The film was grown on aluminum foil at 5 Å/s with a substrate temperature of 200 ^{o}C. This high growth rate typically yields films with a high defect density [12]. Half the sample was then light soaked, with one sun intensity, for 200 hours while the other half remained "as grown". Electron spin resonance (ESR) measurements showed the defect densities for silicon dangling bonds to be on the order of

10^{16} cm^{-3} for the as-grown sample. For the ESR and NMR measurements, the samples were prepared as powders using methods discussed previously [9].

Since hydrogen exists in a variety of environments in *a-Si:H*, each having a unique ^{1}H NMR signature, it is difficult to separate individual components in a typical spectrum. Therefore it is often necessary to use a pulse sequence that can suppress the dominant line shapes with a suitable choice of pulse parameters. As mentioned in the previous section, the three-pulse Jeener-Brockaert (JB) sequence provides such a filtering method [13]. At a time ~ τ_2 after the third pulse, a spin echo forms with the an echo intensity given by

$$I(\tau_1,\tau_2,\tau_{1d}) = I_0(1-e^{-\frac{\tau_1}{T_1}})e^{-2\frac{\tau_2}{T_2}}e^{-\left(\frac{\tau_{1d}}{T_{1d}}\right)^{1/2}}, \qquad (6)$$

where I_o is the initial maximum intensity, T_1 is the spin-lattice relaxation time, T_2 is the spin de-phasing time or spin-spin relaxation time, and T_{1d} is the dipolar spin relaxation time. Henceforth the pulse separations will be denoted as τ_2 and τ_{1d}, and the time over which the three-pulse sequence is repeated will be denoted as τ_1. The utility of this sequence relies on the fact that each hydrogen environment has its own T_2 and T_{1d}. For our purposes, it is also necessary to have either relaxation parameter, T_2 or T_{1d}, longer than those for the more dominant hydrogen environments, which are due to *SiH* that is either randomly placed or clustered in the sample. Since τ_1 characterizes a signal growth, filtering with parameter τ_1 is effective for components with T_1 shorter than those of the dominant sites.

Using the Jeener-Brockaert sequence with parameters {7s, 60μs, 20ms} we obtain in the as-grown sample a line shape displaying a doublet feature with peak-to-peak splitting (Δν) of ~ 16 kHz as shown in Fig. 4. For reference, this figure also contains the line shape found by *Su et al.* [9], which shows a similar doublet feature having Δν ~ 14 kHz. The dashed lines, which serve as aides to the eye, show a qualitative difference in the peak positions. Signatures of the clustered and isolated hydrogen sites (existing as *SiH*) are also present. Past studies have shown these clustered and isolated components contribute to the line shape a Gaussian of ~ *25 kHz* full width half max (FWHM) and a Lorentzian of ~ *4 kHz* FWHM, respectively [14].

Figure 5 shows the doublet line shape for temperatures between 5 and 20 K. Due to the temperature dependence of T_1, we vary τ_1 accordingly to obtain a similar line shape for each temperature. The parameter τ_1 is chosen to be roughly one T_1 for the line-shape components attributed to clustered and isolated *SiH* sites.

Going to longer τ_{1d} suppresses the Gaussian and Lorentzian components thereby yielding a more accurate line shape for the doublet. Figure 3 shows such a trace (bottom trace). In the top trace in Fig. 6 the doublet signal has decayed almost to the noise level, and the remaining two components in the line shape are due to molecular hydrogen (H_2). Shoulders occurring at $\pm$ *90* kHz are characteristic of H_2, which is frozen into the lowest rotational state. The narrow central peak is due to H_2, which exists in thermally excited rotational states [15].

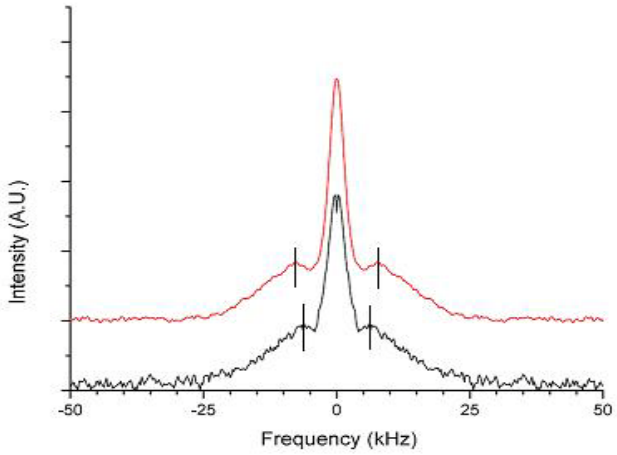

Figure 4. Characteristic line shape for a doublet in two different samples. Shown in the top trace is the as-grown, high-growth-rate sample. The bottom trace is the light-soaked, low-defect-density sample from ref. [9]. Vertical lines are aides to the eye.

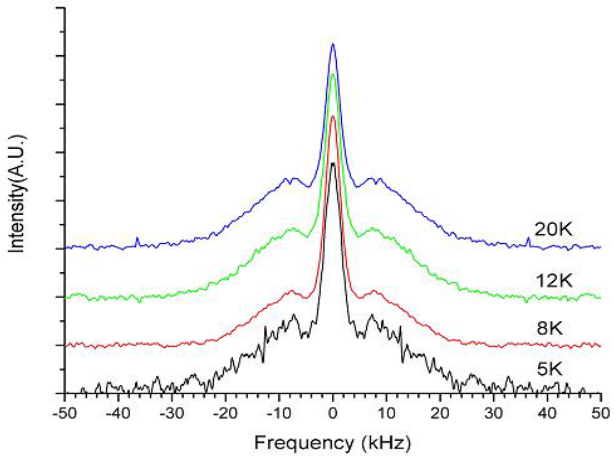

Figure 5. Line shape of ^{1}H NMR at various temperatures. NMR parameters are {1 T_1, 60 μs, 20 ms} for each trace. T_1 values are T_1 = *10s, 8s, 2s, 1s* for *T = 5K, 8K, 12K, 20K*, respectively.

Subtracting the two traces in Fig. 6 yields a good approximation of the doublet line shape. Figure 7 shows the result of this subtraction superimposed on a calculated Pake doublet powder pattern that is broadened by Gaussian of 15 kHz FWHM. The Pake doublet powder pattern is the line shape expected theoretically for an ensemble of paired hydrogen sites that are randomly oriented with respect to the magnetic field. Divergences at ± *14.1* kHz in the de-convoluted powder pattern (not shown) are related to the dipolar coupling constant, which varies inversely as the H-H separation cubed. From the divergences in this particular case, we calculate an *H-H* separation of 1.8 Å.

We note here, that the *real* Fourier transforms of time domain data are shown. Imperfect phase mixing in the quadrature detection scheme, especially for weak signals, results in a *complex* transform that is asymmetric. We stress that the doublet is observed from the *full*

transforms but that the lineshape is distorted in data sets that are not sufficiently well phased mixed.

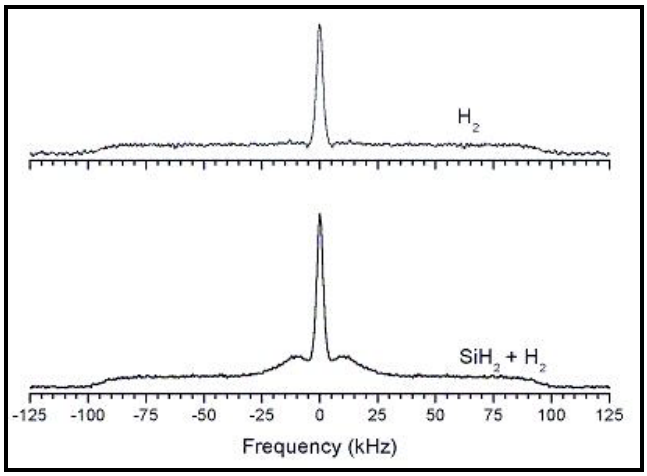

Figure 6. Bottom trace: NMR line shape for {7 s, 60 μs, and 45 ms}. Bonded SiH has decayed leaving only the doublet and H_2. Top trace: NMR line shape for {7 s, 60 μs, and 90 ms}. Only the H_2 signal remains.

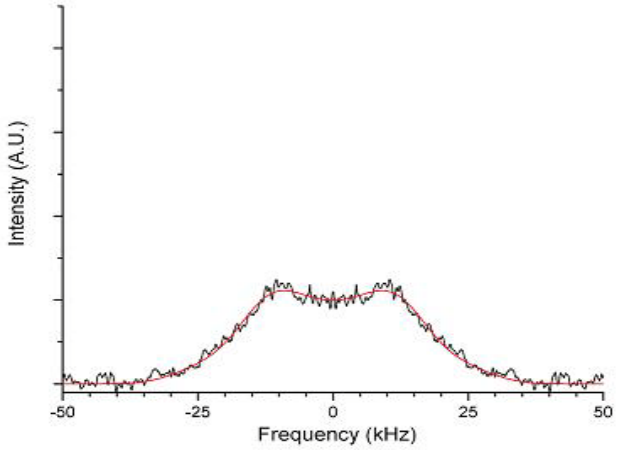

Figure 7. Doublet resulting from subtraction of the two traces in Fig. 6. The smooth line is a calculated Pake doublet powder pattern broadened by a Gaussian of approximately 15 kHz FWHM. See text for details of this calculation.

Besides the qualitatively different peak doublet positions, Fig. 4 suggests that the high-growth-rate sample contains a large density of *H-H* sites (large compared to 10^{-17} cm^{-3}, the density of sites seen by *Su et al.* [8]). To quantify this claim, we have used the NMR methods discussed in [15] to estimate a density of at most 3 *at. %* for this doublet site. Also, we infer a minimum density of ~ 1 *at. %* from vibrational modes observed in Fourier transform infrared spectroscopy. Densities this large, ~10^{21}, suggest that this *H-H* sight is fundamentally different from that found only in light-soaked samples in ref. [9].

The original intent of this work was to investigate in greater detail the metastable hydrogen doublet that accompanies the SWE using a sample, which has a large defect density in the light-soaked state. In this case, the as-grown sample would provide a benchmark line shape for comparison with the light soaked sample. Unfortunately, because of the much smaller density of the metastable doublet sites, we have to date not succeeded in making this comparison. The major complicating fact is the occurrence in the sample of a doublet at much higher densities, and therefore comparisons of the as-grown and light-soaked samples (not shown in this quarterly status report) show no difference in the line shapes. The stable hydrogen doublet site persists in both samples. Therefore, we have concentrated on identifying the hydrogen-hydrogen (H-H) arrangement to determine the *H-H* separation in this site.

To characterize further this different *H-H* site, we have investigated the line shape as a function of the temperature, as shown in Fig. 5. Line shape variations due to motional effects usually exhibit strong temperature dependences due to thermal activation over barriers to the motion. The doublet line shapes in Fig. 5 display no evidence of motional narrowing. Hence we conclude that the doublet consists of hydrogen bonded to silicon.

Definitive identification of the identity of this *H-H* site comes from comparison with infrared spectra. This sample exhibits vibrational modes at 900 cm^{-1} and 850 cm^{-1}, which correspond, respectively, to scissors and wagging modes of SiH_2. Therefore, based on the density of sites, their thermal stability, and their infrared vibrational modes, we attribute the doublet line shape to SiH_2.

In summary, we have made the first detailed NMR measurement of stable SiH_2 in high defect density *a-Si:H*. By filtering out the bonded *SiH* signals, and subtracting the remaining H_2 signal, we obtain the SiH_2 signature: a "doublet" with peak-to-peak splitting of ~ 16 kHz. By considering an isolated SiH_2 with a well-defined *H-H* separation, we calculate 1.8 Å for the *H-H* separation in SiH_2.

b. Si-H Bonding Sites

The implication of hydrogen in the Staebler-Wronski effect (SWE) in hydrogenated amorphous silicon (a-Si:H) has generated enormous interest in understanding the local bonding environments of the hydrogen. In particular, recent proton (^1H) nuclear magnetic resonance (NMR) experiments have linked a specific metastable, "paired" hydrogen site, in which the hydrogen pair is separated by 2.3 ± 0.2 Å, to the SWE [16]. Silicon dihydride (SiH_2) is a possible candidate for this site since calculations using the conventional tetrahedral silicon structure give 2.4 Å as the hydrogen separation [17].

Hydrogen environments can be probed using ^1H NMR techniques because the hydrogen nucleus communicates with the environment through a variety of spin-mediated interactions. In a-Si:H, the dipole-dipole interaction between two protons dominates. For these magnetic dipole interactions, the strength depends strongly on the proton-proton separation. Exciting the system with radiation corresponding to the interaction strength causes the proton system to resonate thereby producing a detectable time varying signal. The resulting Fourier-transformed line shape yields details of the local hydrogen bonding configurations. For instance, by analysis of dipole

broadened line shapes, it has been determined that in a-Si:H bonded hydrogen in the silicon hydride (SiH) configuration exists in both clustered and essentially randomly isolated environments [16].

The SiH_2 line shape exhibits a well-known form resulting from a dipole interaction between two protons. An analytic expression of the intensity of this so-called "Pake doublet" line shape can be expressed in terms of the coupling strength, and hence the proton-proton separation, *r*. It is therefore possible to extract the proton-proton separation by fitting simulated line shapes to the experimental data. This would suffice if the SiH_2 existed as an isolated species with a well-defined *r*. In the case where modulations to the local field exist, due to nearby hydrogen nuclei, the pure Pake doublet is broadened by an amount corresponding to the proximity and number of the nearby nuclei. This "isotropic" broadening effect, which is Gaussian for clustered arrays [18], can be taken as a fitting parameter in subsequent simulations.

Broadening of the pure Pake doublet may also result from a distribution of proton-proton separations. It is known from scattering experiments that the nearest neighbor, Si-Si bond angles vary by ± 10° [19]. Thus it is natural to expect some distribution in *r* that will reflect the amorphous system. The distribution can also be used as a fitting parameter whereby the resulting broadened spectrum is a summation of Pake doublets.

Observation of SiH_2 in low defect density a-Si:H has eluded ^{1}H NMR experiments primarily for two reasons. The first reason is obvious: in device quality films the SiH_2 concentrations are usually below the threshold detection limit of conventional ^{1}H NMR (~ 10^{16} cm^{-3}). Moreover, SiH occurs in concentrations ~ 10^{21} cm^{-3} and therefore dominates the line shape in standard free induction decay (FID) experiments. This fact alone suggests that the FID experiments are insufficient for observing the low concentrations of SiH_2.

A more subtle reason for the lack of experimental observation of SiH_2 in a-Si:H derives from the line shape broadening effects discussed above. Isotropic broadening becomes a problem when it is of the same the magnitude as the resolved dipolar coupling. In this case the Pake doublet is unresolved since its defining features smear to form a nearly Gaussian line shape. For instance, the un-broadened proton dipolar coupling in SiH_2 with r = 2.4 Å is 13.4 kHz [18]. The typical clustered hydrogen environment yields a Gaussian with ~ 25 kHz full width at half maximum (denoted henceforth as σ). Thus there will be no resolved SiH_2 line shape if it exists in an environment that resembles the standard clustered array.

In the present study, we have used ^{1}H NMR to obtain the stable SiH_2 Pake doublet. Simulations of the Pake doublet for various choices of broadening effects were performed. We discuss the simulation details and relevant fitting parameters needed to replicate the experimental data.

The a-Si:H sample used in this study was made at United Solar Ovonic Corporation at high growth rate (5 Å/s). The film was grown on aluminum foil at a substrate temperature of 200 °C. Such samples contain higher defect densities (≥ 10^{17} cm^{-3}) and are generally not suitable for device applications. Fourier transform infrared spectroscopy (FTIR) measurements show IR active modes at 900 cm^{-1} and 850 cm^{-1}, indicative of the scissor and wagging SiH_2 modes,

respectively. The presence of these modes in the FTIR spectrum implies an SiH_2 concentration on the order of 10^{21} cm^{-3} – well above the observation threshold for NMR. For subsequent NMR measurements, the sample was prepared as a powder according to methods previously discussed [16].

For spectral simulations, we numerically compute the "powder pattern" using a method similar to that described by Slichter [20]. The program was built in C++ using the pre-written functions of the GAMMA libraries [21]. For simulations requiring a distribution of r, we chose a Gaussian distribution where σ and mean separation, R_o, are the fitting parameters. Thus the full spectrum resulting from a distribution in r is the summation of individual powder patterns (whose weight depends on the distribution parameters).

Figure 8 shows the frequency domain spectrum of the experimentally obtained Pake doublet with two simulations superimposed. We obtain the experimental Pake doublet by Fourier transforming the time domain signal and subtracting the remaining molecular hydrogen signal. The Zeeman frequency (147.417 MHz) has been subtracted so that the spectral center occurs at 0 Hz. The solid line represents the experimental Pake doublet. For comparison we present the simulated Pake doublets for r = 1.8 Å (peaks at ± 15 kHz) and 2.4 Å (peaks at ± 7 kHz). These simulations are broadened by 1 kHz, but they do not include a distribution of distances. The areas have been normalized to equal that of the experimental data.

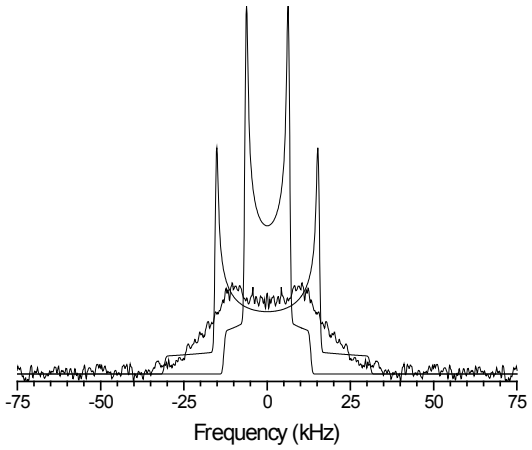

Figure 8. Frequency domain spectrum of the experimental Pake doublet with simulations for r = 1.8 Å (shoulder peaks at ± 15 kHz) and r = 2.4 Å (shoulder peaks at ± 7 kHz). The experimental data were obtained via a Fourier transform of the time domain data and subsequent subtraction of the molecular hydrogen signal. The Zeeman frequency (147.47 MHz) has been subtracted out so that the spectral center occurs at 0 Hz.

Figure 9 demonstrates, in frequency space, the separate effects of isotropic broadening by clustering and by a distribution in r. The top trace represents the unbroadened powder pattern for r = 1.8 Å. Below it, we present a spectrum broadened by 15 kHz (approximately 72% of the dipolar coupling). The bottom trace represents the powder pattern for a Gaussian distribution of

r characterized by the parameters R_o = 1.8 Å, σ = 0.52 Å (30% of R_o). The bottom trace has been further broadened by 1 kHz. Similarities between the broadened spectra suggest that the set of simulation parameters replicating the data is not unique.

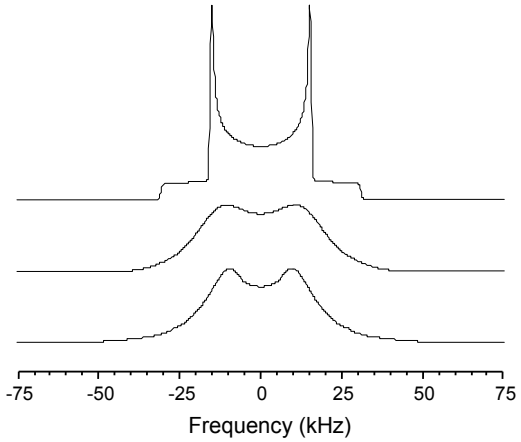

Figure 9. Broadening effects on the simulated Pake doublet for *r* = 1.8 Å. The top trace is a unique Pake doublet broadened by 1 kHz. The middle trace is the Pake doublet for *r* = 1.8 Å (no distribution) with 15 kHz isotropic broadening. The bottom trace represents the Pake doublet simulation for R_o = 1. 8 Å, σ = 0.54 Å, and 1 kHz isotropic broadening.

Figure 10 depicts the simulated spectral fits to the experimental data. The top trace is the simulated Pake doublet for *r* = 1.8 Å, broadened by 15 kHz superimposed on the experimental data. The bottom trace shows the Pake doublet for R_o = 1.8 Å, σ = 0.52 Å broadened by 1 kHz also superimposed on the experimental data. Dashed lines denote the simulated spectra. The experimental data of Fig 8 yield important clues for judicious choices of the fitting parameters. Of the three fitting parameters, the fit is most sensitive to R_o since it varies as r^{-3}. Therefore we first choose R_o according to the qualitative agreement between the unbroadened spectra and experimental data. For *r* = 2.4 Å, the standard result for *r* in SiH_2 according to theoretical calculations [17], there is a clear discrepancy in the shoulder peaks. Since subsequent broadening will only decrease the separation between peaks, it is clear that larger coupling constants (smaller *r*) are favored. With *r* = 1.8 Å, the shoulder peaks occur just outside of the experimental Pake doublet and serve as a good candidate for R_o.

In accounting for the broadening effects, we note that the resolved peaks in the data require the total broadening to be less than the coupling constant—20.6 kHz for *r* = 1.8 Å. Two broadening mechanisms are available and hence any combination of the two satisfying the overall broadening requirement will yield a suitable fit. The NMR data are insufficient to answer the question of uniqueness. However, by mimicking the clustered and isolated environments known to exist for SiH (see for instance [17]), we deduce limits on the range of acceptable parameters.

We obtain the first limiting case by assuming that SiH_2 exists in hydrogen-clustered regions of the amorphous network. We also place the constraint that there exists a well-defined *r* = 1.8 Å

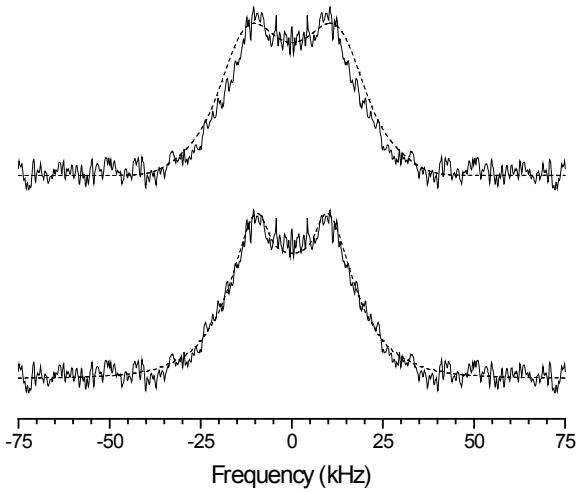

Figure 10. Simulated Pake doublets superimposed on the experimental data. The dashed line in the top trace shows the simulation fit r = 1.8 Å (no distribution) with 15 kHz isotropic broadening. The dashed line in the bottom trace shows the simulation fit for R_o = 1. 8 Å, σ = 0.54 Å, and 1 kHz isotropic broadening

for the SiH_2 sites. This seems unreasonable in light of the known nearest neighbor bond angle variation [19]. In the clustered region, the SiH_2 is isotropically broadened. The effect of 15 kHz of isotropic broadening is shown as the middle trace in Fig. 9. We present the fit to the data as the dashed line in the top trace of Fig. 10. The resulting spectrum sits outside the shoulders in the data—a discrepancy that may be accounted for by minor adjustments in R_o and the amount of isotropic broadening.

By imitating the isolated environment of SiH, we obtain the second limiting case. It is known, from hole burning experiments, that isolated SiH sees ~ 1 kHz broadening due to the surrounding hydrogen nuclei [18]. Thus we take this as our isotropic broadening parameter. To complete the broadening, we include a Gaussian distribution of r. The resulting spectrum with parameters R_o = 1.8 Å and σ = 0.54 Å is shown as the bottom trace of Fig. 2. The bottom trace of Fig. 10 shows the near perfect fit of these simulations to the data. Simulations with R_o = 1.9 Å and 1.7 Å have yielded inferior fits to those presented.

As demonstrated in Fig. 10 the true SiH_2 environment cannot be inferred directly from the NMR results. In either limiting case, R_o = 1.8 Å is the essential ingredient. Thus in light of prior ^1H NMR results linking a paired hydrogen site with r = 2.4 Å to the SWE, it is unlikely that an "average" SiH_2 site is involved. However, if the true r distribution includes this value, we cannot rule out SiH_2 as a candidate. Therefore, if the metastable, paired hydrogen site that stabilizes the SWE is indeed a SiH_2 site, then it must be a rare embodiment that is not indicative of the average site.

In summary, we have fitted the experimental Pake doublet for stable SiH_2 with line shape simulations whose fitting parameters reflect the local environment and variation in proton-proton separations. Accurate fits of the data are available for fitting parameters that imitate the clustered and isolated SiH environments. We take these sets of fitting parameters as the limiting cases whereby the true SiH_2 environment is a mixture of the two. We find for both extremes that an accurate fit is obtainable only when the proton-proton separation in SiH_2 is on average 1.8 Å. Hence a distribution of proton-proton separations is necessary if SiH_2 is to be involved with the SWE.

IV. Hydrogen-Hydrogen Separation at Silicon Dihydride Bonding Sites in a-Si:H

The hydrogen bonding environments and their correlation to film quality have been the subject of an enormous body of research; see for example ref. [19]. It is generally believed that a more ordered a-Si:H matrix leads to smaller void structures and therefore to improved opto-electronic properties. As such, the concentration of large polysilane hydrogen structures, such as $(SiH_2)_n$, is thought to be small compared to the total hydrogen content for device quality films. IR studies seem to support this trend; higher quality films show no evidence of the $(SiH_2)_n$ scissor or wagging modes near 800-900 cm^{-1}. Most of the hydrogen is bonded to silicon and can be found either in clusters, such as on the internal surfaces of voids, or in isolated regions of the matrix. Since these sites occur in sufficient quantity, >1 atomic percent (at. %), they can be detected via their IR modes near 2000 cm^{-1}. Below the IR sensitivity of approximately1 at %, the hydrogen bonding structures cannot be observed, and hence the $(SiH_2)_n$ content is unknown.

We have discussed above (previous section) the ^1H NMR spectra of $(SiH_2)_n$ in a high defect density film. At these sites the average hydrogen-hydrogen separation is 1.8 Å [22]. In this section we describe similar $(SiH_2)_n$ structures in as-grown, higher quality material where the IR modes are absent. Of course, *n* may be unity for these sites; i.e., isolated silicon dihydride sites. Using ^1H NMR, which is a more sensitive probe of the bonded hydrogen, we have estimated the $(SiH_2)_n$ content for both films. We compare estimates of the $(SiH_2)_n$ content. Contrary to current belief, we find a significant fraction of the total hydrogen content can be bonded in $(SiH_2)_n$ configurations in "device quality" films supplied by United Solar Ovonics. The film has a dark-to-photo conductivity ratio of 10^{-5}. IR absorption measurements show no evidence of the 800-900 cm^{-1} wagging or scissor modes characteristic of $(SiH_2)_n$.

The film produced at United Solar that we discussed in the previous section was intentionally grown at a high deposition rate by PECVD. As a result, a high defect density (mid 10^{17} defects cm^{-3}) film was produced that contained observable 800-900 cm^{-1} IR wagging or scissor modes. From the total intensity of these modes compared to the total 600 cm^{-1} absorption intensity due to bonded silicon monohydride, we estimate that the hydrogen occurring in the $(SiH_2)_n$ configuration is approximately 10% of the total hydrogen. It is generally accepted that the 600 cm^{-1} absorption region contains contributions from all silicon bonded hydrogen sites [23,24]. Therefore, we take 10% as an estimate of the total hydrogen bonded in the $(SiH_2)_n$ form.

The growth conditions for both films are summarized in Table 1. Results reported in this section are for the as-deposited films that have not been subjected to deliberate light soaking.

To probe the signal decay of each hydrogen component, we used the Jeener-Brockaert three-pulse sequence. Details of the pulse sequence and its utility in studying hydrogen bonding in a-Si:H can be found in ref. [25]. In this particular application, we measured the stimulated echo decay as a function of the time separation between pulse pairs. In general, the total signal amplitude, I_T, can be written as:

$$I_T(\tau_2,\tau_{1d}) = \sum_i I_{io} e^{-2\frac{\tau_2}{T_{i2}}} e^{-\left(\frac{\tau_{1d}}{T_{i1d}}\right)^{1/2}} \qquad (7)$$

where I_{io} represents the initial maximum intensity for the ith component (for a discussion of the usual line shapes, see ref. [26]), T_2 is the characteristic decay time due to spin de-phasing, and T_{1d} is the dipolar spin relaxation time. Pulses 1 and 2 are separated by τ_2 (typical values are tens of μsec) while pulses 2 and 3 are separated by τ_{1d} (tens of msec typically). We determine these parameters separately by measuring the decay of the intensity as a function of τ_2 (τ_{1d}) when τ_{1d} (τ_2) is kept constant.

When the decay times are known, the total maximum intensity for each component is computed by correcting the signal intensity, at any time, with the appropriate exponential arguments given in Eq. 7. This procedure amounts to extrapolating the component signal intensity to zero time. The total signal and the relative concentrations of any component, C_i, are then computed by:

$$I_T(\tau_2 = 0, \tau_{1d} = 0) = \sum_i I_{io} \quad \text{and} \quad C_i = \frac{I_{io}}{I_T(\tau_2 = 0, \tau_{1d} = 0)} \ . \qquad (8)$$

Experimentally, it is quite difficult to obtain perfect line shape fits. The spectral features can be artificially distorted by imperfections in the detection scheme. As a result, the fits can lead to intensity mismatches that, in turn, affect the error reported in any one component. Since the measurement relies on an extrapolation of an exponential function, small uncertainties are compounded at τ_2 , $\tau_{1d} = 0$. There is also uncertainty in the total intensity incurred from the signal to noise ratio of each measurement. Our measurements are reported using the combined, additive effects of these uncertainties. This procedure yields a more conservative error estimate than the standard quadrature rules of error propagation.

Because no doublet features are observed in the NMR spectra obtained at τ_2 and $\tau_{1d} = 0$ (the free induction decay), an upper bound on the concentration of $(SiH_2)_n$ sites is estimated by calculating the total NMR frequency spectra with varying contributions from all known components. Figure 11 (bottom trace, solid line) demonstrates one such composite line shape that results when the spectra in the upper plot are added in concentrations of (top to bottom, respectively) 15%, 15% and 70%. When the percentages are 30%, 30%, and 40%, respectively, the doublet is no longer resolved. The top trace of the upper plots is a Lorentzian, corresponding to the isolated SiH and characterized by a full width at half maximum (FWHM) of 4.2 kHz. Immediately below it is a Gaussian with a FWHM of 25 kHz, which represents the clustered SiH. A simulation of the Pake doublet, where the average hydrogen-hydrogen splitting is 1.9 Å is drawn immediately below the Gaussian. This spectrum is characteristic of two strongly interacting hydrogen atoms as would occur for atoms in the $(SiH_2)_n$ configuration [22]. The percentages are representative of the minimum $(SiH_2)_n$ contribution necessary to achieve the resolved peaks near ±10 kHz shown in the bottom trace. The doublet peaks in Fig. 11 help to distinguish it from the other components that mask the doublet's intensity. When these two features are present, the component concentrations can be more accurately determined.

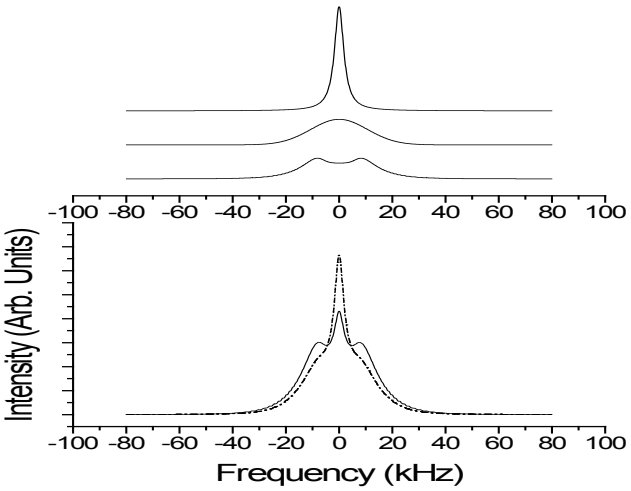

Figure 11. Estimate of the minimum ^{1}H NMR signal intensity needed to observe $(SiH_2)_n$. Top: Normalized ^{1}H NMR signals of (top to bottom) isolated SiH, clustered SiH, and $(SiH_2)_n$. Bottom: Signal resulting from addition of differing amounts of the three components. Solid line: 15% isolated SiH, 15% clustered SiH, and 70% $(SiH_2)_n$. Dashed Line: 30% isolated SiH, 30% clustered SiH, and 40% $(SiH_2)_n$

Table 1. Summary of $(SiH_2)_n$ concentration measured from NMR and IR. The reported value is the percent concentration relative to the total hydrogen concentration observable by NMR and IR. "Min %" refers to the minimum concentration estimate, within experimental uncertainty. Details of the growth conditions are also provided.

Sample	Min % $(SiH_2)_n$ NMR Estimate	% $(SiH_2)_n$ IR Estimate	Growth Conditions (films grown by PECVD)			
			Substrate Temp (^{o}C)	Growth Rate (Å/sec)	Power (mW/cm^2)	Pressure (mTorr)
United Solar (high quality)	12	No Modes	200	**2**	50	500
United Solar (low quality)	15	10	200	**5**	50	500

Figure 12 shows the decay of the intensity, for the 4 components, as a function of τ_{1d} when $\tau_2 = 60$ μsec. The data have been scaled such that the extrapolation to $\tau_{1d} = 0$ msec is 100. The data are plotted on a log scale vs. $(\tau_{1d})^{1/2}$ so the extrapolation to $\tau_{1d} = 0$ can be evaluated by inspection. The dashed lines, drawn as aides to the eye, enclose the $\tau_{1d} = 0$ $(SiH_2)_n$ concentrations allowed by experimental uncertainties. The upper (lower) bound occurs near 70% (10%) of the total signal intensity. The combined Lorentzian and Gaussian contributions are plotted, since they have essentially the same T_{1d}. At $\tau_{1d} = 1$ msec, the total Lorentzian and Gaussian components comprise essentially all of the total intensity.

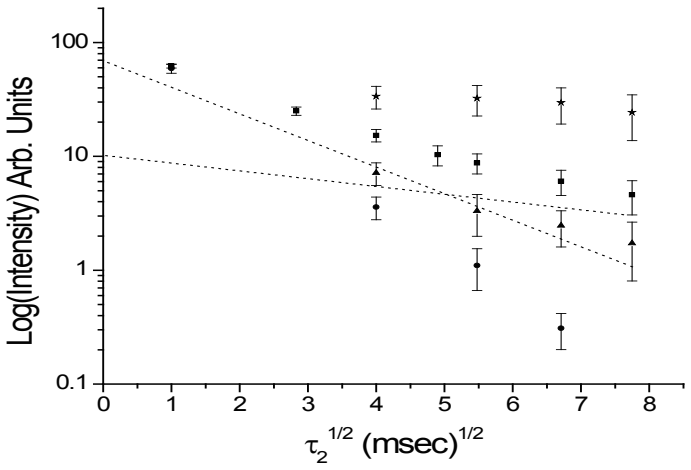

Figure 12. Log of the signal intensity as a function of $(\tau_{1d})^{1/2}$. For all data points, τ_2 = 60 μsec. "▪" represent total signal intensity, "▲" represent the $(SiH_2)_n$ intensity , "★" represent the H_2 x 10 intensity, and "●" represents the clustered and isolated SiH signal intensity. Dashed lines are aides to the eye. These two dashed lines enclose the possible $(SiH_2)_n$ signal intensities for τ_{1d} = 0 msec as allowed by experimental uncertainty.

Figure 13 shows the decay of the total intensity as a function of τ_2, when τ_{1d} = 1 msec for an a-Si:H sample grown under the same conditions as those listed in Table 1. The data are again scaled to read 100 at τ_2 = 0 μsec. There are two distinct decay regions, as indicated by the lines. The fast (slow) decay region has $T_2 \cong 60$ μsec ($\cong 300$ μsec). These T_2 values correspond, respectively, to the Gaussian and Lorentzian components.

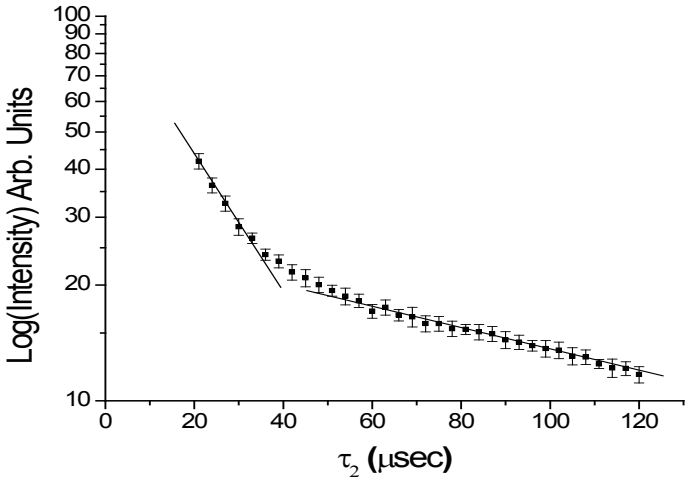

Figure 13. Log of the total signal intensity as a function of τ_2 (τ_{1d} = 1 msec for all data points) for a typical a-Si:H film. The solid lines are aides to the eye and indicate the values of T_2 for the clustered and isolated SiH. For the clustered SiH, $T_2 \cong 60$ μsec. The isolated SiH has a $T_2 \cong 300$ μsec.

The data in figs. 12 and 13 are sufficient to determine the component concentrations from Eq. 8. Since T_2 is directly related to the component line width, we take 60 μsec as an approximation of T_2 for the $(SiH_2)_n$. The specific $(SiH_2)_n$ bonding environment and distribution of hydrogen-hydrogen separations is presently unknown and hence a more accurate evaluation of T_2 is unavailable. Using T_2 = 60 μsec to correct for the τ_{1d} = 0 msec $(SiH_2)_n$ signal intensity, we calculate a minimum relative $(SiH_2)_n$ concentration, $C_{(SiH2)n}$ = 12 %. In the same calculation, about 70 % of the total hydrogen is in the clustered configuration, 15 % exists in the isolated phase, and 1 % exists as ortho-H_2 (para-H_2 has total spin of 0 and is unobservable by NMR).

The existence of a minimum 12 % $C_{(SiH2)n}$ in the higher quality film is a bit surprising in light of the large body of NMR research on a-Si:H. However, Fig. 11 shows that $(SiH_2)_n$ must contribute a considerable fraction (~ 70 %) to the total spectrum before its features can be distinguished from the usual line shapes. If we take this as an upper bound on $C_{(SiH2)n}$, then the $(SiH_2)_n$ spectrum would not be observed by conventional free induction decay, or solid echo NMR techniques. The actual concentration of hydrogen in $(SiH_2)_n$ sites is clearly less than 70 % since no definitive evidence of $(SiH_2)_n$ from these conventional methods has been reported. As the dashed lines in Fig.11 demonstrate, the combined Gaussian and Lorentzian line shapes can mask a considerable fraction of $(SiH_2)_n$.

We have previously made similar measurements of $C_{(SiH2)n}$ in a high defect density sample of a-Si:H. The growth conditions are provided in Table 1. The NMR measurements of $C_{(SiH2)n}$ yield a range between 15 % and 60 %, consistent with $C_{(SiH2)n}$ estimates based on IR data. Within the NMR experimental error, $C_{(SiH2)n}$ can be the same for both films or, at most, differ by a factor of 6. To be consistent with the IR data for the defective film, the higher quality $C_{(SiH2)n}$ can be at most equal to the minimum detectable signal in the IR measurements. In either case, the $(SiH_2)_n$ densities differ by less than an order of magnitude in these two films.

Concentration measurements from NMR can clearly be used as a more sensitive probe of hydrogen bonding sites than the standard IR measurements. This NMR analysis will undoubtedly be useful in future film characterizations, if specific hydrogen sites are related to the metastabilities commonly observed in a-Si:H. Presently, the role of $(SiH_2)_n$ in any metastability is unclear, and a correlation between the $(SiH_2)_n$ concentration and film quality has yet to be established.

In summary, we have compared the concentration of hydrogen in $(SiH_2)_n$ sites occurring in higher quality and high defect density a-Si:H films. Our results show that, despite the large difference in film quality, the hydrogen concentrations in $(SiH_2)_n$ sites are within an order of magnitude of each other. We have shown that when compared to the usual silicon bonded hydrogen sites, 40% of the total hydrogen content can exist in $(SiH_2)_n$ structures before being visible by conventional nuclear magnetic resonance methods.

V. Calculations of Silicon Dihydride Bonding Sites in a-Si:H

In 1977 Staebler and Wronski reported a fundamental experiment on hydrogenated amorphous silicon (a-Si:H) [27], which revealed marked decreases in both the dark and photoconductivities after light soaking. Subsequent work showed that light soaking created

defects, most probably dangling bonds. Because hydrogenated amorphous silicon (a-Si:H) is a material with technological applications, understanding the phenomenon of light-induced degradation, i.e., the Staebler-Wronski effect (SWE), has been a major focus [28]. In the intervening thirty years, extensive work in experiment and modeling has been carried out to obtain the microscopic origin and fundamental understanding of light-induced degradation. Disorder in the network, hydrogen concentration and its complex bonding structure, and concentrations of impurities are some of the material properties that play a role in the SWE. We have reported an experimental clue of some importance [16] where we performed nuclear magnetic resonance (NMR) experiments on protons in a-Si:H and found that the NMR spectrum of light-soaked a-Si:H films shows the preferential creation of a hydrogen doublet where the H-H distance is 2.3 ± 0.2 Å. This experiment appears to directly connect light soaking to creation of a specific new structure (or family of structures) in the amorphous matrix. In our collaborative efforts with the group at the Ohio University, we have shown that SiH_2 is a possible candidate for the observed proton separation. Zhang, Jackson, and Chadi [29] and Chadi [30] have shown in careful calculations in c-Si:H that a two H interstitial complex, H_2^{**}, is another potential candidate for the observed defect. Both proposals have the merit that they do not rely on an unlikely conformation found only in specific models, and appear to occur with significant reproducibility, consistent with the reasonably well-defined experimental distance.

There have been various proposals for the microscopic origins of the SWE. One class of models involves breaking of "weak bonds" whose microscopic properties are often unspecified [31]. Another class of models proposes the creation of new defects as a result of movement or diffusion of an original defect [32]. Zafar and Schiff [33] considered a metastability model based upon transfer of H between clustered and isolated phases seen by NMR. Bonding in each of these phases was presumed to be monohydride. In their subsequent work Zafar and Schiff showed that the 2-phase picture closely accounted for experiments on thermal changes in the spin-density and also the changes caused by evolving hydrogen [34]. Some current theories combine the electronic and hydrogen energy states and hydrogen diffusion as in the hydrogen collision model of Branz [35], and the hydrogen flip model of Biswas and Li [36]. Kopidakis and Schiff [37] have proposed that clustered-phase sites can bind either one or two hydrogen pairs (dihydride bonding). Using this line of argument, Zhang and Branz [38] proposed a model that vacancies that produce missing Si atoms, at which the remaining Si atoms are fully terminated with Si-H bonds eliminate DB's and strained Si-Si bonds and provide the paired-H reservoir and metastability sites in a-Si:H. There are also new findings that reveal a lack of spatial correlation between the defects and hydrogen, the realization that the effectiveness of light induced defects as recombination centers depends on the light exposure conditions, and the observation that it is not only defects that are produced by extended light exposure but also larger structural changes in the material involving the Si network [28].

There are two possible interpretations of our previous NMR results [16]. The simplest interpretation is that some metastable, paired-hydrogen site, perhaps, but not necessarily SiH_2, is formed after the exposure to light. A second interpretation, which cannot be ruled out by the experiments to date, is that some changes in the various NMR relaxation rates after exposure to light allow existing paired-hydrogen sites, such as SiH_2, to become observable in the NMR spectra. Of particular importance to the latter interpretation, Stutzmann, Jackson, and Tsai [31] have argued that the breaking of weak Si-Si bonds will also promote the diffusion of dangling

bonds away from their original sites. If the presence of such a dangling bond near a stable, paired-hydrogen site, for which the most logical candidate is SiH_2, allows this site to be seen in the H NMR, then the results of Su et al. are also logically explained. Although there are technical reasons why this explanation is not as probable as the formation of metastable, paired-hydrogen sites, it cannot be ruled out. The simulations in collaboration with the Ohio University group support either of these two interpretations.

In these simulations we used the *ab initio* code, SIESTA [39,40,41], within the local density approximation (LDA). Details of these simulations are available elsewhere [42].

The calculations began with a defect-free 64-atom a-Si model [43] and removed two Si atoms and added 8 H atoms to create defect-free (that is, gap state free) structures with SiH_2 present. This model is denoted as aSiH-70. Another model is obtained in the same way except that one more Si atom is removed to form aSiH-72 (61 Si atoms and 11 H atoms), which includes one dangling bond [44]. This supercell surgery was repeated at other sites to generate an ensemble of models to obtain some insight into the bonding statistics of SiH_2 conformations in the solid state. The SiH_2 confirmations obtained in the two models are shown in Fig. 14(a) and Fig. 14(b). Four configurations were considered for each model in our calculation. Each configuration in the respective models was constructed by selecting different (typically tetrahedral) sites of the SiH_2 conformations in the cell. Calculations of the SiH_2 structures and dynamics on each of the four configurations of the aSiH-70 model and also on each of the four configurations of the aSiH-72 model were performed. The system was then relaxed. Details of the relaxation procedures are available elsewhere [42]. There is a consistent pattern that in the amorphous matrix the proton-proton separation is significantly reduced relative to a gas phase silane molecule with tetrahedral bonds (which produces a separation of 2.45 Å).

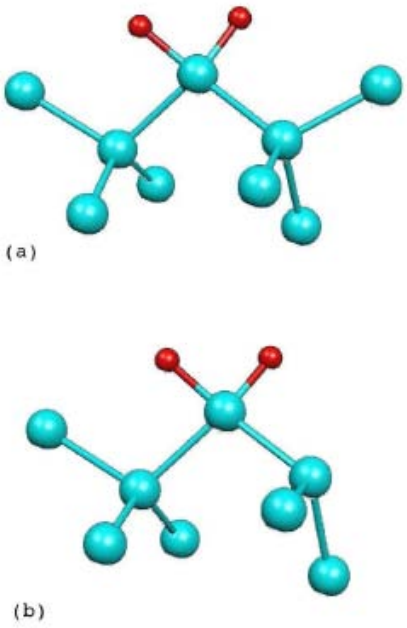

Figure 14. (a) SiH2 conformation in aSiH-70 model and (b) SiH2 conformation in aSiH-72 model with a dangling bond. In the figure the hydrogen atoms are shown in red (smaller in size) and the silicon atoms are shown in cyan (larger in size).

Thermal molecular dynamics (MD) simulations were performed to estimate the H-H distance at room temperature and to compare to T=0. The cells evolved freely for 250 fs (within a time step of 0.05 fs) at a temperature of T = 300 K. Thermal fluctuations in the bond lengths were observed as indicated in Fig. 15(a), and from Fig. 15(b). Over 5000 step MD runs, the average H-H distance becomes 2.41 Å in the case of the LDA calculations and 2.34 Å for the GGA calculations for an initial H-H distance of 2.27 Å.

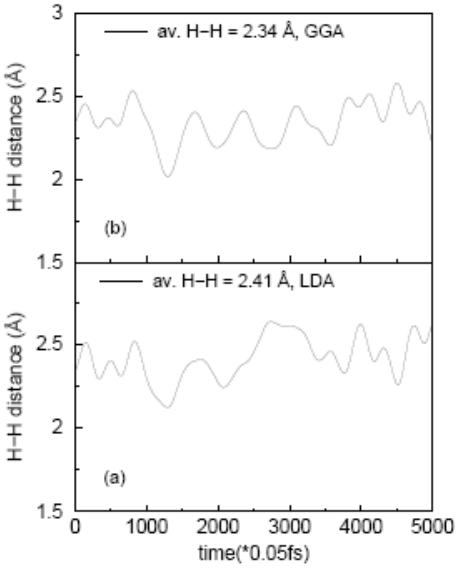

Figure 15. Thermal MD simulation for the H-H distance in aSiH-72 model using a) LDA calculations and b) GGA calculations [36].

The same calculation has also been done for the aSiH-72 model. Consistent with the first configuration, the aSiH-72 model also gives proton separations well within the tolerance of the experiments of Su et al. [16].

Most of the aforementioned models of the SWE invoke paired-hydrogen sites. These models associate the SWE with the conversion of isolated H into paired-hydrogen sites, for which SiH_2 must be considered a prime candidate. The experiments of Su et al. [16] provide direct evidence that light soaking creates structures with a proton-proton separation of about 2.3 Å. Given the remarkably well-defined nature of the observed proton separation, it is natural to expect that the structure(s) causing the feature must not be a very rare conformation. Something like the complex of Chadi [30], or the SiH_2 proposal presented here, appear to fulfill that condition – one certainly expects a priori that both of these configurations should occur in a-Si:H, although it is not initially obvious with what probability.

Given that the various models proposed [24−38] all appear to be at least consistent with our calculations for SiH_2, the link between these calculations and the NMR experiments could be a very important step. On the other hand, what has not been done is to provide any explanation of the light-induced formation of SiH_2, which is certainly a key missing piece to the puzzle. This is not an easy process to simulate, since the (diffusive) time-scales for creation are presumably vastly longer than what is directly accessible from our simulation.

In summary, using accurate methods and supercells properly representing the disorder of a-Si:H, we have seen that SiH_2 is a credible candidate for the proton-proton distance inferred from the work of Su et al. [16]. The results indicate clearly that rather accurate methods are needed to properly describe the bonding in this system.

VI. Defects in Tritiated a-Si:H

a. Growth of ESR and PDS at 300 K

The most important metastable effect in the prototypical amorphous semiconductor, hydrogenated amorphous silicon (a-Si:H), is the so-called silicon dangling bond defect associated with a threefold coordinated silicon atom. It is this defect that is thought to control the decreases in the conductivity and photoconductivity that occur due to exposure to visible light. These changes are collectively known as the Staebler-Wronski effect [45], which is the major factor in determining the stability of photovoltaic devices and detectors made from a-Si:H.

In this section we describe recent results using a novel method for producing silicon dangling-bond defects by replacing some of the hydrogen ^{1}H with tritium ^{3}H. When the tritium, which is radioactive and decays to ^{3}He with a half-life of approximately 12 years, is bonded to silicon its decay leaves behind a silicon dangling bond and an inert helium atom. [Tritium decays to helium-3 emitting an antineutrino and a beta particle with an average energy of 5.7 keV]. The great advantage of this method for producing silicon dangling bonds is that one can calculate accurately the number that is produced as a function of time.

For many years hydrogen diffusion has been invoked to explain the kinetics for the production and annealing of the Staebler-Wronski effect [46-54]. Although there is recent evidence that hydrogen pairing plays a role in stabilizing the Staebler-Wronski defects [55], the assumption of significant diffusion of hydrogen at room temperature is supported only by circumstantial evidence. In addition, there has been speculation for many years that the Staebler-Wronski effect involves the creation of far more extensive changes in the local structural order [56] than might be expected from the simple production of a small number (approximately 10^{17} cm^{-3}) of silicon dangling-bond defects. In this section we provide direct evidence for the diffusion of hydrogen to heal the production of a large density (approximately 10^{21} cm^{-3}) of silicon dangling bonds. Some of the diffusion might be essentially athermal and occur even at very low temperatures. Together these two results – the diffusion of hydrogen and the annealing of a large density of silicon dangling bonds – greatly enhance our understanding of the Staebler-Wronski effect, which is the quintessential metastability in all of the tetrahedrally coordinated amorphous semiconductors. Our results have a major impact on the two classes of models [51, 52] that have been proposed to explain the Staebler-Wronski effect because both classes invoke the motion of only a small density of hydrogen atoms, about one per defect created, to stabilize the defects.

We present results on two samples, deposited by plasma-enhanced chemical vapor deposition (PECVD) from SiH_4 and tritium gas mixtures, under conditions described elsewhere[57]. The first sample was grown at a substrate temperature of 225 ^{o}C. This sample is similar to those used in devices, in which the initial defect densities are the lowest experimentally obtainable (film thickness of 0.26 μm). The second sample was grown at 150 ^{o}C. This sample, which is representative of a more defective material (film thickness of 1.5 μm), showed considerable dihydride bonding (silicon bonded to two Si and two H atoms) as measured by Fourier transform infrared (FTIR) spectroscopy. Because of the presence of silicon-tritium

bonds, one expects the tritium decay to accumulate Si dangling bond defects after the samples have been deposited. The density of these defects should follow approximately the number of decayed tritium atoms per unit volume. Since our first measurements were made seven years after deposition, the density of decayed tritium was about $6x10^{20}$ cm^{-3} or a few at. %. Surprisingly, both electron spin resonance (ESR) measurements of the neutral silicon dangling bond density and photothermal deflection spectroscopy (PDS) measurements of the absorption of both neutral and charged defects yielded densities that were lower by about 3 orders of magnitude (5 x 10^{17} cm^{-3} and 4 x $10^{17}$$cm^{-3}$ for films deposited at 150 ^{o}C and 225 ^{o}C, respectively). In addition, most of these defects annealed at temperatures between about 150 and 200 ^{o}C with kinetics similar to that observed for the optically induced defects created in the Staebler-Wronski effect. The residual spin densities in the samples after annealing at the highest temperatures, near the deposition temperatures, were 9 x 10^{16} cm^{-3} and 2 x 10^{16} cm^{-3} for samples deposited at 150 and 225 ^{o}C, respectively. For the film deposited at 225 ^{o}C, Fig. 16 shows the fraction of metastable defects that remains after 30 min at several stepwise annealing temperatures, T_A (open circles). The defect densities are normalized to their saturated values before annealing. This annealing behavior is quite similar to annealing of the optically induced defects in non-tritiated PECVD a-Si:H, performed at the University of Chicago [58] at room T for a week and stepwise annealed afterwards. The similarity of the annealing curves for tritiated and non-tritiated samples suggests similar distributions of defect annealing energies.

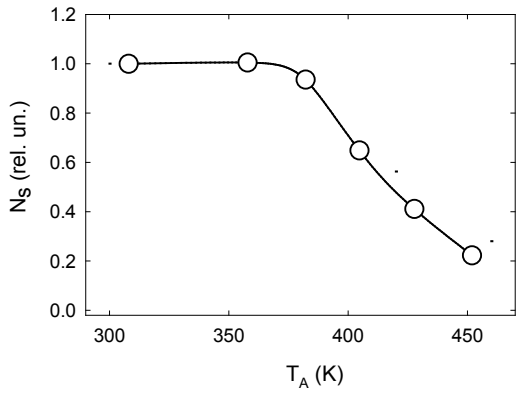

Figure 16. Fraction of defects, N_S, remaining after stepwise annealing for 30 min at each temperature T_A . Open circles represent the annealing of a tritiated sample of a-Si:H made at a substrate temperature of 225 ^{o}C and stored 7 years at room temperature (MRS 2004).

After the final annealing, new defects begin to accumulate in these tritiated samples in the dark. The accumulation kinetics depends on the temperature at which the samples are stored. Figures 17 and 18 show the number of newly created defects as functions of time after the final annealing for the samples grown at 225 ^{o}C and 150 ^{o}C, respectively. Data are shown for the accumulation of defects at 25, 77, 300, and 353 K (the last temperature is only shown for the sample grown at 150 ^{o}C). PDS measurements were performed for the samples kept at room temperature. Because the sample deposited at 225 ^{0}C was only 0.26 μm thick, a considerable portion of the spin density in the annealed state is likely due to surface or interface defects [52, 59]. Therefore, the annealed spin density was subtracted from the total spin density to get the

concentrations ΔN_S of newly created defects shown in Figs. 9 and 10. The large scatter in the 300 K data at short times in Fig. 17 is indicative of the inherent error in the measurements.

Figure 17. Kinetics of the accumulation of new defects, ΔN_S, after annealing at 180 °C in a sample of tritiated a-Si:H deposited at 225 °C. Open circles and triangles represent ESR measurements on the sample kept at 77 K and 25 K, respectively. Solid symbols indicate the same sample kept at room temperature, with the solid circles and diamonds representing ESR and PDS measurements, respectively. The dashed curve is a linear fit to the 77 K data, and the solid curve show the calculated number of tritium decays in the sample after the annealing. The measurement error in ΔN_S is approximately ±2 x 10^{16} cm^{-3} (MRS 2004).

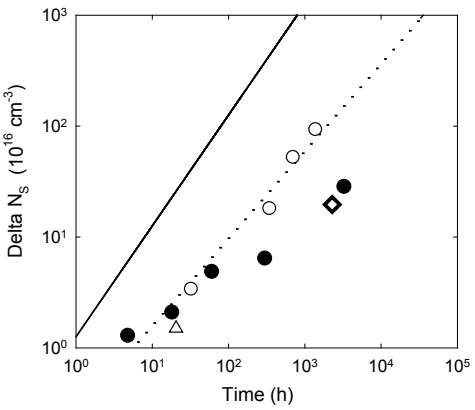

Figure 18. Kinetics of the accumulation of new defects after annealing at 150 °C in a sample deposited at 150 °C. The symbols represent same quantities as those described in the caption to Fig.2. The solid line is the calculated tritium decay (1.7x10^{16} cm^{-3}/h), and the dashed line is a linear fit to the 77K data. Large and small solid circles denote two separate experiments at room temperature. The relative error in ΔN_S is about 5x10^{15} cm^3. (MRS 2004).

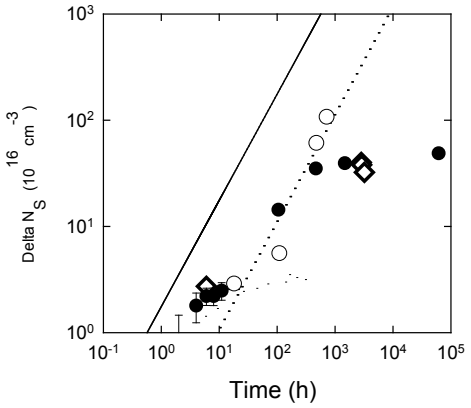

Two distinct features are apparent from the data in Figs. 17 and 18. At short times the growth is nearly linear, within experimental error, but much slower than the estimated production of silicon dangling bonds. Therefore the first general feature is that the initial growth rate is essentially independent of temperature (athermal) over the entire range of temperatures studied. At the higher temperatures (300 K and above) the defects accumulate more slowly at longer times and eventually saturate, and the saturated densities increase with decreasing temperature consistent with the data shown in Fig. 16. At 300 K the growth roughly follows a stretched exponential rise to a saturation that occurs after approximately 10^4 hours in the sample grown at 225 °C and at shorter times (and higher densities) in the sample grown at 150 °C. This behavior is very similar to that which is observed under optical excitation. In contrast, when the sample is kept at 77 K, there is no sign of saturation even after 10^4 hours. Therefore, the second general feature is a saturation level, which is strongly temperature dependent. If these saturation levels are thermally activated, they suggest an activation energy of approximately 0.3 eV.

Because the nuclear reaction for tritium decay also creates an energetic electron (beta particle) and a much less energetic ^{3}He, we must first rule out any annealing (or generating)

effects of these two particles. The ^{3}He has a recoil energy of only a few eV, which is unlikely to have much effect in either annealing or generating defects. The electrons are emitted with an average energy of approximately 6 keV, and the average distance they travel through the film is approximately 0.6 μm. During this process each electron produces about 10^3 electron-hole pairs, which can in principle generate additional defects; however, this production rate of electron-hole pairs is equivalent to illumination by only about 10^{-6} W/cm^2 of visible light, which implies the production of about one defect for 50 electrons [60]. This production rate is too small to be of any consequence.

It is conceivable that the energetic electrons locally heat up the lattice in such a way as to anneal defects, but calculations suggest that the probability is low. Nonetheless, we tested this defect annealing hypothesis by exposing the film grown at 225 ^{o}C, after saturation of the defect density, to a 7 keV electron flux in an electron microscope. The average incident current density was 10^{-8} A/cm^2 and the exposure time was 1.5 h. This flux is about 200 times larger than the effective beta particle flux, which bombards any small volume element in the film (~ 10^{-11} A/cm^2). Thus, the 1.5 h e-beam exposure is equivalent to 10 days of intrinsic beta particle exposure. In the saturated steady state, the annealing rate is equal to the defect creation rate of about 10^{16} cm^{-3} h^{-1}. If the beta particles were responsible for annealing of defects, we would see a decrease of the saturated defect density by about 10^{18} cm^{-3} after the e-beam exposure, but we observed no measurable change. We conclude that the emission of beta particles (energetic electrons) during the decay of tritium has no significant influence on the production or annealing of defects in tritiated a-Si:H.

In addition, it is conceivable that there is a large density of positively and negatively charged defects that are unseen by ESR. Figs. 17 and 18 show clearly that this is not the case at room temperature; here the defect densities measured by PDS (optical absorption), which is believed to measure both neutral and charged defects, match those measured by ESR. At 25 and 77K, the growth of the ESR signal is remarkably similar to that seen at short times at room temperature, which strongly suggests that charged defects are not important at any temperature.

It remains to explain the two general features of the growth curves – an annealing of defects at short times that is essentially athermal, and an annealing at long times (saturation) that is strongly temperature dependent. Because we have tested the saturation over time scales approaching seven years, this feature requires a significant reservoir of hydrogen sites on the order of an atomic percent. In a typical sample of a-Si:H, such as our tritiated one grown at 225 ^{o}C, there is approximately 10 at. % hydrogen that ^{1}H nuclear magnetic resonance (NMR) measurements show [61, 62] exists in three primary forms: ~ 7 at. % bonded to silicon in small clustered environments, ~ 3 at. % bonded to silicon at isolated (randomly distributed) sites, and ~ 1 at. % interstitial molecular hydrogen (H_2), of which approximately half is HT (hydrogen-tritium) and one quarter is T_2 (tritium-tritium) in the tritiated sample.

The most obvious candidate to provide the mobile hydrogen necessary for annealing [63] is the decay of hydrogen–tritium (HT) or T_2 molecules, which leaves behind an unbonded H (or T). It is unlikely that molecular hydrogen is the only source given the very different temperature dependences for the short-time and long-time annealing processes and the need for a very large reservoir of potential hydrogen sites. A second possible candidate is the replacement of two near neighbor bonds in the clustered phase [64] (e.g., Si-H and Si-T) with silicon-silicon bonds on

formation of a silicon dangling bond by tritium decay. This reconstruction eliminates the newly created Si dangling bond and at the same time, produces an extra H (or T) atom that can easily diffuse and passivate another defect nearby.

The low rates of defect production in the linear regime show there is some tritium decay that does not produce defects: some athermal process circumvents this defect production. Either the diffusion of at least some of the hydrogen is athermal or the replacement of some of the silicon-hydrogen bonds with silicon-silicon bonds, as discussed above, is athermal. The latter appears to be the more likely possibility if the lattice relaxation is strong enough at the clustered H sites. This explanation requires that the H produced in the same process has no ESR signal. With this mechanism, the metastable defects are created essentially at the isolated tritium sites, which represent only a fraction of the total tritium sites. Thus, tritium decay produces both Si dangling-bond defects at isolated tritium sites and "mobile" hydrogen at clustered tritium and hydrogen sites. In the saturation regime at higher temperatures, the hydrogen released at clustered sites can thermally diffuse to passivate defects. Saturation is possible when the annealing rate due to diffusion of interstitial hydrogen is equal to the defect production rate.

What are the implications of these results for understanding the Staebler-Wronski effect in a-Si:H? The similarity of the annealing of the defects induced by tritium decay and the optically induced defects at room temperature (Fig.16) suggests that the annealing in both cases is likely to be governed by the same mechanism. The annealing of light-induced defects has been extensively studied and is characterized by a wide distribution of annealing activation energies [52, 65]. There is much circumstantial evidence that the annealing of optically induced defects is mediated by mobile hydrogen [50, 66]. Both classes of model for the Staebler-Wronski effect suggest [51, 52] that defect annealing is mediated by a metastable configuration that is created together with the defects and can reverse the creation process during anneal. In both models, however, only a small density (10^{17} cm^{-3} in device quality films) of such metastable species is created after prolonged optical excitation. In the tritiated samples, however, the tritium bonded to silicon is converted into inert ^{3}He and therefore plays no role in the formation of metastable configurations capable of annealing Si dangling bond defects. As discussed above, the metastability must be mediated by hydrogen from a large reservoir of *already existing* metastable sites (a few at. %). As no new defects are created by the tritium decay at these metastable sites, an isolated Si-H could not fill this role, but molecular hydrogen and clustered hydrogen bonded to silicon could. We therefore conclude that the annealing of optically induced defects that are created in the Staebler-Wronski effect at room temperature and elevated temperatures might also take place from a large, pre-existing reservoir of annealing species rather than from stabilization mechanisms of a small density of defects that are created by the light.

Finally, we address the growth of defects created by tritium decay and those created by optical excitation at temperatures below 300 K. The optically induced defect densities are difficult to measure at low temperatures by ESR [67] or by the constant photocurrent method [56, 58], but neither of these experiments has observed saturation at temperatures much below 300 K. Unless the presence of optical excitation plays a role in the saturation process, one can speculate that the behavior at low temperatures is similar to that observed in the tritiated samples.

Some of the network healing mechanisms, which follow tritium decay, are essentially athermal and occur even at very low temperatures.

b. Growth of ESR at 77 K

The appearance of optically or electrically induced defects in hydrogenated amorphous silicon (a-Si: H), especially those that contribute to the Staebler-Wronski effect [68], has been the topic of numerous studies, yet the mechanism of defect creation and annealing is far from clarified. This quarterly status report describes our recent progress using another method to induce silicon dangling-bond defects by replacing some of the hydrogen, ^{1}H, with tritium, ^{3}H. Tritium decays to ^{3}He, emitting a beta particle (average energy of 5.7 keV) and an antineutrino. This reaction has a half –life of 12.5 years. The samples contain approximately 7 and 10.4 at.% tritium. In these tritium-doped a-Si: H samples each beta decay will create a defect by converting a tritium, which is bonded to silicon, to an interstitial helium, leaving behind a silicon dangling bond.

We have tracked these defects through electron spin resonance (ESR) and photothermal deflection spectroscopy (PDS) [69]. The densities we measured at room temperature were smaller by orders of magnitude than the number of tritium decays – only about $5x10^{17}cm^{-3}$. Therefore, there must exist a mechanism of defect annealing that is capable of healing ~ 10^{20} cm^{-3} defects at room temperature. In the present report, we extend these studies to 77K, in order to establish the thermal stability of the Si dangling bond defects introduced by tritium decay.

Both samples studied were made at the University of Toronto in 1996. The samples used in this experiment were deposited at glass substrate temperatures of 150ºC (further referred to as G181) and 225 ºC (referred to as G83). Shortly after deposition high temperature tritium effusion experiments determined the tritium concentration to be approximately 7 and 10 at. % in the two samples, respectively.

We expect the tritium decay to accumulate Si dangling bond defects because of the silicon-tritium bonds. The density of these defects is related to the number of tritium atoms that have decayed per unit volume. We first measured the samples 7 years after deposition, where the density of tritium atoms that had decayed since making the films was about $6x10^{20}$ cm^{-3} [69]. However, both ESR and PDS measurements of the defect densities were lower by about 3 orders of magnitude because the defect density saturates at room temperature [69]. Next, we annealed the samples near the deposition temperature and kept the two samples at liquid nitrogen temperature for almost two years. During this time we used ESR to track the defect densities. After two years, the defect densities were about 10^{19} cm^{-3} for both samples. After two years in liquid nitrogen, we annealed the two samples. We step-wise annealed the G83 sample at successive temperatures up to 473 K isochronally while the G181 sample was annealed isothermally at 300 K.

After annealing the films, the defects began to accumulate in the dark at 77 K. The spin densities as functions of time stored at 77K are shown in Figs. 19 and 20 for the samples G181 and G83, respectively. The data at the shortest times are the defect densities just after annealing. These densities are about 10^{16} cm^{-3} and 10^{17} cm^{-3} for G181 and G83, respectively. In both cases, the densities are probably due to surface or interface defects. The spin densities increase linearly with time. The final data points are the defect densities after about two years. In Fig.19, the final density is about $3x10^{19}$ cm^{-3}, which is about 4 times lower than $1.4x10^{20}$ cm^{-3}, the density of

tritium atoms, which have decayed since the sample was annealed. In Fig. 20, the final density is about $2x10^{19}$ cm^{-3}. In both samples there is no saturation in the growth in contrast to the case at 300 K. [69].

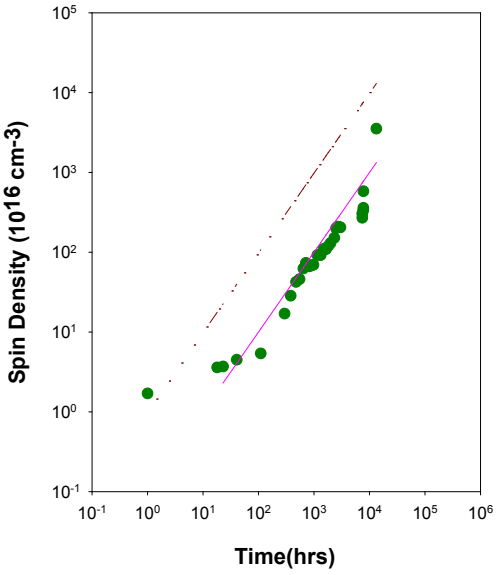

Figure 19. Increase of the defect densities of G181 as a function of time at 77 K. (MRS 2007)

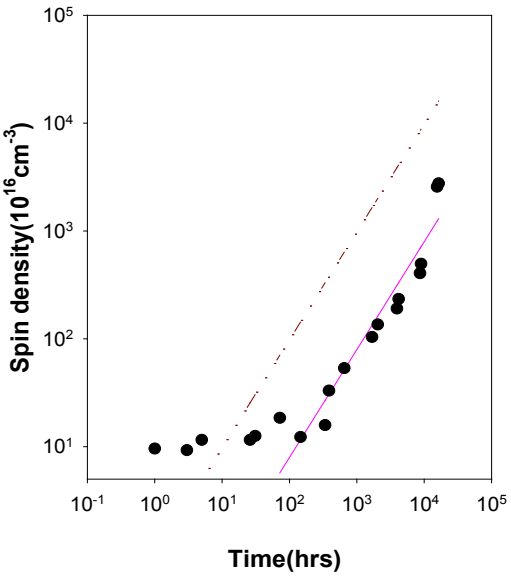

Figure 20. Increase of the defect density of G83 as a function of time at 77 K. (MRS 2007).

Figure 21 shows the decrease in defect densities after sample G181 was heated to room temperature and then kept at room temperature for several months. The defect densities were tracked by ESR. At 300 K the defects created at 77 K anneal slowly. Even after several months, the density is still higher t han the saturation density for defects created at room temperature, which is $6x10^{17}$ cm^{-3}. Only after about one year does the defect density reach the saturated value at 300 K[2]. Because PDS measures both charged and uncharged defects in the sample, we used this technique to check that the ESR was measuring all of the defects. The densities of defects, as measured by ESR in these samples of a-Si: H, are the same as those measured by PDS within a factor of two.

Figure 22 shows data for stepwise annealing of the G83 sample up to 380 K. The sample was kept for 30 minutes at each annealing temperature, T_a. We continued annealing step by step up to 380 K, and after each annealing step we measured the spin densities at 20 K. The data show that the defects are fully annealed at 473 K. The final density of approximately 10^{17} cm^{-3} matches the number after we annealed the sample at the start of the 77 K experiments.

At 77 K the defects accumulate almost linearly with the time. The spin density after two years is smaller than the density of tritium atoms that have decayed. This result possibly suggests that the tritium decay in a clustered hydrogen environment does not produce a dangling bond due to bond reconstruction as a result of emission of hydrogen from nearly Si atom. This

suggestion is similar to the previous suggestion of thermal emission of hydrogen from the clustered phase [70, 74]. In addition, some tritium decays do not produce a silicon dangling bond because the tritium occurs in molecular form (trapped $^{1}H^{1}H$ or ^{3}H-^{3}H). The sample G83

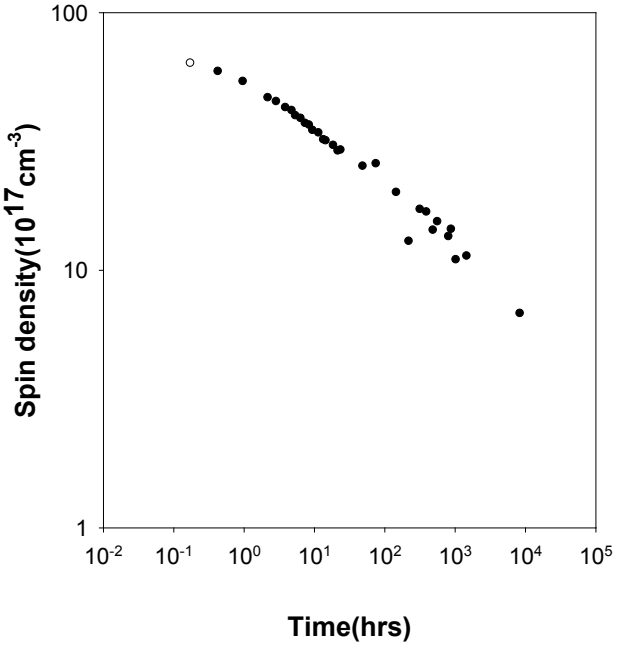

Figure 21. Decrease in the defect density after the sample G181 was heated to room temperature and then kept at room temperature for several months of isothermal annealing. (MRS 2007)

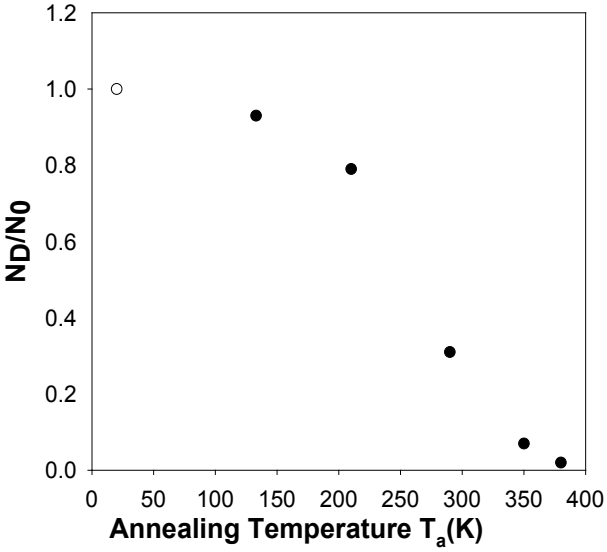

Figure 22. Relative decreases in defect density in sample G83 after stepwise annealing for 30 minutes at each successive annealing temperature, T_a. (MRS 2007).

was annealed step-by-step up to 200 ºC. Annealing results are similar to those that are observed when defects are created with light (Staebler-Wronski effect) at low temperatures. Two thirds of the defects are annealed at around 300 K in our tritium sample. In some a-Si:H samples light soaked at 77 K essentially the same annealing kinetics is observed [71, 72].

In summary, we have shown that the defect densities of two tritiated amorphous silicon samples at 77 K increase linearly in time up to 10^{19}cm^{-3}. The final densities, however, are factors of 4 to 8 smaller than the density of tritium atoms that have decayed. From NMR experiments, we know that 3 at. % of the atoms in the sample exists as hydrogen in the dilute phase and the rest is in the clustered phase [76]. Therefore, some of the clustered tritium atoms probably do not produce silicon dangling bonds at 77 K due to reconstruction. There is no evidence of saturation at 77 K. These results provide further hints for the role of hydrogen in creating defects in light soaked samples at low temperature as suggested in [73-75].

VII. Hydrogen Diffusion and Crystallization

We have investigated the evolution of the defects created during hydrogen effusion and the crystallization process, using magnetic resonance techniques such as nuclear magnetic resonance (NMR) and electron spin resonance (ESR). In this section, we show the results from ESR during the annealing and crystallization and present a simple model of the exchange interaction in the disordered *a*-Si.

Amorphous silicon samples were deposited by both HWCVD and PECVD at the facility at National Renewable Energy Laboratory (NREL). Information of the samples is listed in Table 2. One HWCVD sample (H2029) and one PECVD sample (L1477) were annealed at the same time at $T = 560^{\circ}C$ in nitrogen gas. A second PECVD sample was annealed at $T = 580^{\circ}C$ for 1300 min, and reflectance measurements show that the film crystallized after $t \sim 1050$ min. The annealing is monitored by a n&k reflectance and transmittance spectrometer.

Table 2. Growth conditions of the HWCVD and PECVD *a*-Si:H samples.

Sample #	Deposition method	Substrate temperature (°C)	Deposition rate (Å/s)	Thickness (μm)
L1447	PECVD	250	1-2	~1
H2029	HWCVD	400	7	~1

ESR measurements of the defect densities were carried out on a Bruker Elex 500 Spectrometer at room temperature. The defect densities were obtained by comparing the double integrated intensity in the samples to that in a standard weak pitch sample measured under the same conditions.

Figure 23 shows the evolution of the defect densities in H2029 and L1477 as a function of the annealing time at $T = 560^{\circ}C$. In the HWCVD sample (H2029), the defect density begins to decrease after about 60 min, and the film is fully crystallized after about 750 min. Reflectance measurements show that crystallization occurs during the same time period. After the film is

crystallized, the defect density deceases to about 4×10^{17} cm^{-3} and remains at this value through the rest of the annealing.

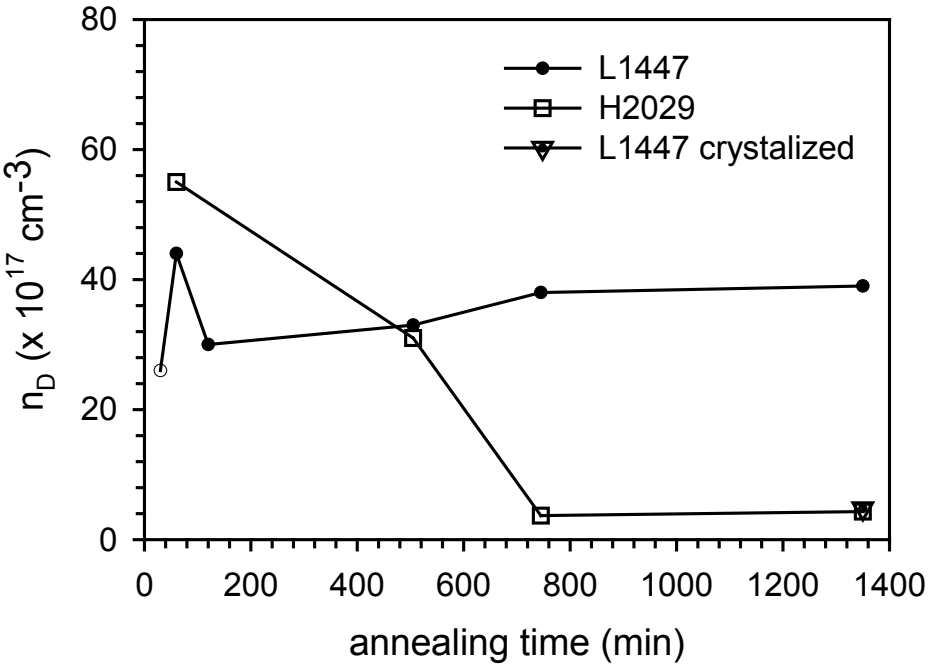

Figure 23. The defect densities in HWCVD (H2029) and PECVD (L4774) samples as a function of annealing time at $T = 560^{\circ}C$. Open squares and solid circles indicate data for HWCVD and PECVD samples, respectively. The open triangle indicates defect the density of the PECVD sample after annealing at $T = 580^{\circ}C$ for *t*~1300 min.

The defect density in PECVD sample (L4774) shows an initial sharp increase to about 4×10^{18} cm^{-3}, followed by a decease to 3×10^{18} cm^{-3}, and a gradual increase over the remainder of the annealing. This sample does not show any evidence of crystallization, which is consistent with the reflectance measurements. Due to the lack of detailed data on the HWCVD sample, we will focus our discussion in the PECVD sample.

Figure 24 shows the comparison of the lineshapes of the ESR signals in H-effused and crystallized samples to that in a typical *a*-Si:H sample. In trace (a), which is from a typical *a*-Si:H sample, the peak-to-peak width is about 7 G. Trace (b) is from the sample in the H-effused state before crystallization, the line-width is about 5 G. The line-width of the crystallized sample (6.5 G) is much smaller than previously reported values in micro-crystalline silicon (μc-Si:H) samples [77, 78, 79]. The lineshape changes can be attributed to exchange-narrowing that is well known for high defect density films [80]. This narrowing effect will be discussed in detail later. Figure 24 also shows a slight difference in the g-values as calculated from the field of zero crossing, which could be due to the difference in ESR resonance frequency or to a slight change in *g*-value of the defect signal.

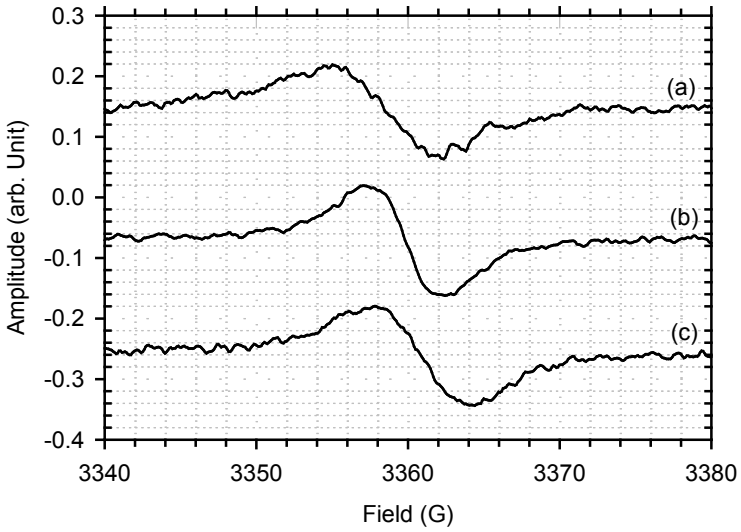

Figure 24. Comparison of the ESR lineshapes in H-effused and crystallized samples to a typical *a*-Si:H sample. (a) typical a-Si:H, (b) H-effused, before crystallization ($n_D = 3.6\times10^{18}$ cm^{-3}), and (c) after crystallization ($n_D = 4.3\times10^{17}$ cm^{-3}). The amplitudes are scaled to show the difference in line-width.

Since only the total number of spins is measured in typical ESR spin count measurements, these measurements do not determine whether or not the spins are clustered. The bulk defect density is only accurate based on the assumption that the defects are randomly distributed within the sample. This is unlikely during the crystallization, as well as right before and after crystallization. To investigate the potential clustering of the spins, we compared the lineshape in the hydrogen effused PECVD sample to that in an a-Si:HT sample. In a-Si:HT, the defects are crested by decay of the tritium toms that are bonded to silicon atoms,

$$^3\text{H} \text{ --> } ^3\text{He} + \beta^- + \text{anti-neutrino} + 5.7 \text{ keV} \qquad (9)$$

The resulting ^{3}He atom will detach from the silicon atom and leave a dangling bond on the Si atom. The energy of the β particle is ~ 5.7 keV. Irradiating the sample with an electron beam with the same energy and dosage shows that no significant amount of defects are created [81, 82]. Therefore the main mechanism for defect creation is due to the reaction in Eq. (9). This process does not involve large-scale lattice reconstruction, due to the slow decay rate of the tritium nuclei, and therefore this process presumably creates defects that are more likely to be randomly distributed. Figure 25 shows the dependence of the line-width on the defect densities in one *a*-Si:HT sample. For comparison, the line-width of the H-effused PECVD sample with a bulk defect density of $n_D = 3.6\times10^{18}$ cm^{-3} and the line-width in an *a*-Si sample prepared by RF sputtering [80] are also shown.

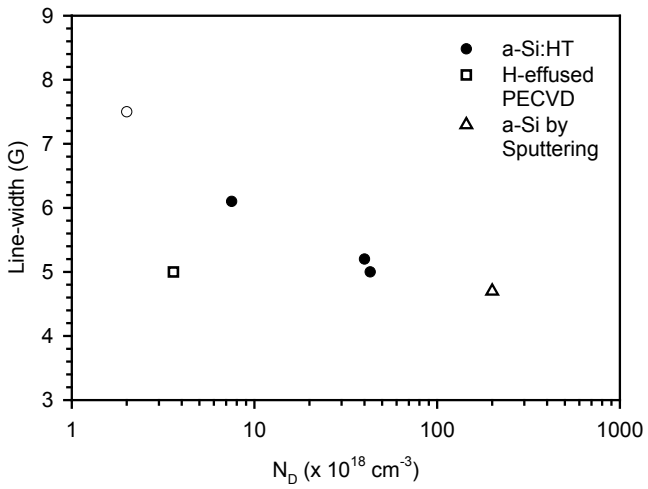

Figure 25 The dependence of the ESR line-width on the defect densities in *a*-Si:HT sample and in H-effused *a*-Si:H sample prepared by PECVD. Solid circles represent the data from the *a*-Si:HT sample, the open square represents the line-width for the defect density of $n_D = 3.6 \times 10^{18}$ cm^{-3} in the H-effused PECVD sample. The open triangle is the line-width from Ref. [80] in *a*-Si sample prepared by RF sputtering.

Figure 25 clearly shows the discrepancy in line-width between the H-effused PECVD sample and the *a*-Si:HT sample with the same bulk defect density. The defect density in *a*-Si:HT is about one order of magnitude higher with the same line-width (~5 G). If we assume the defects are randomly distributed in *a*-Si:HT, then there must be significant clustering in the H-effused sample to have a comparable line-width, with a much lower bulk defect density. This result will be further discussed below.

It is well known that at high spin densities, the observed ESR line-width is narrower due to the so-called exchange-narrowing effect [83]. This effect arises from the exchange interaction between the spins, and has the form

$$H_{ex} = J\vec{S}_1 \cdot \vec{S}_2 \ , \qquad (10)$$

where $\vec{S}_1$ and $\vec{S}_2$ are the spins of the two defects. J is the coupling constant. This interaction allows the spin-pair to undergo rapid mutual flipping and effectively average out the broadening due to other interactions, such as the dipole-dipole interaction between the spins and g-tensor anisotropy. The exchange interaction deceases rapidly as the distance between the two spins increases, and therefore this interaction does not affect the line-width at low spin densities. Although this effect has been extensively studied in crystalline materials, no details to estimate the coupling constant have been reported. Here we develop a rather simple method to estimate the interaction in *a*-Si:H.

Consider two defects (dangling bonds) that are separated by n Si atoms. In this case, the exchange-interaction will be through the n-1 bonds in between. The dangling bond, which is a singly occupied sp^3 hybrid on a Si atom, interacts with another dangling bond by coupling to the Si-Si bond on the same atom, which in turn couples to another Si-Si bond, and so on. If we only

consider the coupling through the bonding orbitals, the matrix of the total Hamiltonian is an $(n+1)\times(n+1)$ matrix,

$$\begin{pmatrix} 0 & \frac{V_1}{\sqrt{2}} & 0 & \cdot & \cdot & \cdot & 0 \\ \frac{V_1}{\sqrt{2}} & -V_2 & \frac{V_1}{2} & \cdot & & & \cdot \\ 0 & \frac{V_1}{2} & \cdot & \cdot & \cdot & & \cdot \\ \cdot & \cdot & \cdot & \cdot & \cdot & \cdot & \cdot \\ \cdot & & \cdot & \cdot & \cdot & \frac{V_1}{2} & 0 \\ \cdot & & & 0 & \frac{V_1}{2} & -V_2 & \frac{V_1}{\sqrt{2}} \\ 0 & \cdot & \cdot & \cdot & 0 & \frac{V_1}{\sqrt{2}} & 0 \end{pmatrix} \tag{11}$$

where $\frac{V_1}{\sqrt{2}}$ is the coupling between the dangling bond and the Si-Si bond, $\frac{V_1}{2}$ is the coupling between two hybrids within a bond, and V_2 is the energy gained by forming the bonding orbital. Diagonalization of this matrix results in n+1 energy levels, of which n-1 levels are close to V_2 (bonding orbitals). The other two energy levels are higher and are separated only by a small energy, which is due to the exchange interaction between the two dangling bonds.

To estimate the onset of the exchange-narrowing of the lineshape, we assume that the narrowing will be measurable when the exchange interaction is about the same as the line-width of the ESR signal. By choosing V_1 = 1.8 eV and V_2 = 4.4 eV for Si [84], we numerically diagonalized the Hamiltonian (Eq. 11), and obtained a value of the exchange interaction of $\Delta E_{ex} = 5.4\times10^{-8}$ eV when the two dangling bonds are separated by 12 atoms. This value of ΔE_{ex} corresponds to an ESR line-width of about 4.6 G. The defect density is calculated to be about 3×10^{19} cm^{-3}, with an average distance between two defects of 12 inter-atomic distances of Si. This is consistent with the experimentally observed relation between defect density and the ESR line-width in *a*-Si:HT, in which we assume the defects are randomly distributed, and not significant clustered.

We found that ΔE_{ex} decreases exponentially with an increasing number of bonds between the two dangling bonds. Therefore, the exchange interaction is effectively a short-range interaction. As a consequence, our results do not distinguish between the case in which more than two defects are close to each other and the case in which only paired defects are present.

In summary, we have performed ESR measurements in H-effused *a*-Si:H thin films made by both HWCVD and PECVD. The evolution of the defect density as a function of annealing time is consistent with that found in optical measurements. Analysis of the line-width shows that in H-effused states, the defects are either clustered or exist in pairs. A simple model of the exchange interaction in *a*-Si can account for the difference in line shapes observed in these films as compared to *a*-Si:HT samples described in the previous section.

VIII. Summary

During the sub-contract we have made significant progress in understanding the metastable, hydrogen-doublet defect that may be responsible for stabilizing the silicon dangling bond defects that occur during optical excitation (Staebler-Wronski effect). Also, we have made the first definitive measurement of the H-H separation at silicon doublet bonding sites in a-Si:H. These sites are probably not silicon dihydride but rather hydrogen atoms on nearest neighbor silicon atoms on the surfaces of voids. Also, we have discovered some interesting features concerning the production and annealing of silicon dangling bonds by studying their creation through the decay of tritium in tritiated samples of a-Si:H. We have made significant progress in understanding the role of SiH_2 in both high and low defect-density films of a-Si:H. In addition, we have calculated the H-H separation at SiH_2 sites that may be consistent with that observed in NMR light-soaking experiments. Finally, we have studied annealing and crystallization in films of a-Si:H.

REFERENCES

1. T. Su, P. C. Taylor, G. Ganguly, and D. E. Carlson, Phys. Rev. Lett. **89**, 015502 (2002).
2. D. E. Carlson, K. Rajan, and D. Bradley, in *Proc. 26th IEEE Photovoltaic Specialists Conf.* (IEEE, New York, 1997) pp. 595.
3. J. Jeener and P. Broekaert, Phys. Rev. 157, 232 (1967).
4. T. Su, S. Chen, P. C. Taylor, R. S. Crandall, and A. H. Mahan, Phys. Rev. B **62**, 12849 (2000).
5. J. B. Boyce and S. E. Ready, Physica B **170**, 305 (1991); J. B. Boyce, S. E. Ready, M. Stutzmann, and R. E. Norberg, J. Non-Cryst. Solids, **114**, 211 (1989).
6. L.R. Lichty, J-W. Han, R. Ibanez-Meier, D. R. Torgeson, and R. G. Barnes, Phys. Rev. B **39**, 2012 (1989).
7. M. Stutzmann, W. B. Jackson, and C. C. Tsai, Phys. Rev. B **23**, 23 (1985).
8. H. M. Branz, Phys. Rev. B **59**, 5498 (1999)**.**
9. T. Su, P.C. Taylor, G. Ganguly, and D.E. Carlson, Phys. Rev. Lett. **89**, 015502 (2002).
10. Tesfaye A. Abtew, D. A. Drabold, and P. C. Taylor, Appl. Phys. Lett. **86**, 241916 (2005).
11. P. Gupta, V. L. Colvin, and S. M. George, Phys. Rev. B **37**, 8234 (1988).
12. J. C. Knights, and G. Lucovsky, *CRC Critical Reviews in Solid State and Materials Science* **21**, 211.
13. J. Jeener and P. Broekaert, Phys. Rev. **157**, 232 (1967).
14. J. A. Reimer, R. W. Vaughn, and J.C. Knights, Phys. Rev. B **24**, 3360 (1981).
15. T. Su, S. Chen, and P. C. Taylor, Phys. Rev. B **62**, 12849 (2000).
16. T. Su, P.C. Taylor, G. Ganguly, and D.E. Carlson, Phys. Rev. Lett. 89, 015502 (2002).
17. Tesfaye A. Abtew, D. A. Drabold, and P. C. Taylor, Appl. Phys. Lett. 86, 241916 (2005).
18. J. A. Reimer, R. W. Vaughn, and J.C. Knights, Phys. Rev. B 24, 3360 (1981).
19. R. A. Street, *Hydrogenated Amorphous Silicon,* Cambridge University Press, Cambridge, England, (1991).
20. C. P. Slichter, *Principles of Magnetic Resonance*, Springer Series in Solid-State Sciences, Springer Verlag, 3rd enlarged and updated ed., Jan. (1990).

21. S.A. Smith, T.O. Levante, B.H. Meier, and R.R. Ernst, *J. Magn. Reson.*, **106a**, 75-105, (1994).
22. D. C. Bobela, T. Su, P. C. Taylor and G. Ganguly, J. Non. Cryst. Sol., 2006, *in press*.
23. M. H Brodsky, Manuel Cardona, and J. J. Cuomo, Phys. Rev. B **16**, 3556 (1977).
24. W. B. Pollard, and G. Lucovsky, Phys. Rev. B **26**, 3172 (1982).
25. T. Su, S. Chen, and P. C. Taylor, Phys. Rev. B **62**, 12849 (2000).
26. W. E. Carlos, and P. C. Taylor, Phys. Rev. B **26**, 3605 (1982).
27. D. L. Staebler and C. R. Wronski, Appl. Phys. Lett. **31**, 292 (1977).
28. H. Fritzsche, Annu. Rev. Mater. Res. **31** 47-79 (2001).
29. S. B. Zhang, W. B. Jackson and D. J. Chadi, Phys. Rev. Lett. **65** 2575 (1990).
30. D. J. Chadi, App. Phys. Lett. **83** 3710 (2003).
31. M. Stutzmann W. B. Jackson and C. C. Tsai, Phys. Rev. **B 32** 23 (1985).
32. R. Biswas, I. Kwon and C. M. Soukoulis, Phys. Rev. **B 44** 3403 (1991).
33. S. Zafar and E. A. Schiff, Phys. Rev. **B 40** 5235 (1989);
34. S. Zafar and E. A. Schiff, Phys. Rev. Lett. **66** 1493 (1991); ibid. J. Non-Cryst. Sol. 137-138 323 (1991).
35. H. M. Branz, Phys. Rev. **B 59** 5498 (1999).
36. R. Biswas and Y. -P. Li, Phys. Rev. Lett. **82** 2512 (1999).
37. N. Kopidakis and E. A. Schiff, J. Non-Cryst. Sol. **266-269** 415 (2000).
38. S. B. Zhang and Howard M. Branz, Phys. Rev. Lett. **87** 105503 (2001); for a recent review see H. Branz, Solar Energy Materials and Solar Cells **78** 425 (2003).
39. P. Ordej´on, E. Artacho and J. M. Soler, Phys. Rev. **B 53** 10441(1996).
40. D. S´anchez-Portal, P. Ordej´on, E. Artacho and J. M. Soler, Int. J. Quantum Chem. **65** 453 (1997).
41. J. M. Soler, E. Artacho, J. D. Gale, A. Garc´ıa, J. Junquera, P. Ordej´on and D. S´anchez-Portal, J. Phys.: Condens. Matter **14** 2745 (2002).
42. T. A. Abtew, D. A. Drabold, and P. C. Taylor, Appl. Phys. Lett. **86**, 241916-1 (2005).
43. G. T. Barkema and N. Mousseau, Phys. Rev. **B 62** 4985 (2000).
44. This second conformation reveals only that the proton-proton distances reported are "robust" even for a rather different chemical environment. It is unlikely that the SiH2 would be so close to a dangling bond. See S. Yamasaki, H. Okushi, A. Matsuda, K. Tanaka and J. Isoya, Phys. Rev. Lett. **65** 756 (1990).
45. D. L. Staebler and C. R. Wronski, Appl. Phys. Lett. **31**, 292 (1977).
46. R. A. Street, Hydrogenated Amorphous Silicon (Cambridge Univ. Press, 1991).
47. P. V. Santos, N. M. Johnson and R. A. Street, Phys. Rev. Lett. **67**, 2686 (1991).
48. D. E. Carlson, Appl. Phys. A-Mater. Sci. Process. **41**, 305 (1986).
49. W. B. Jackson and S. B. Zhang, In: Transport, Correlation, and Structural Defects, ed. by H. Fritzsche (World Scientific, Singapore, 1990), p. 63.
50. W. B. Jackson and J. Kakalios, Phys. Rev. **B37**, 1020 (1988).
51. H. M. Branz, Phys. Rev. **B59**, 5498 (1999).
52. M. Stutzmann, W. B. Jackson and C. C. Tsai, Phys. Rev. **B32**, 23 (1985).
53. A. Asano, Physica B **170**, 277 (1991).
54. J. Shinar, R. Shinar, X. L. Wu, S. Mitra and R. F. Girvan, Phys. Rev. **B43**, 1631 (1991).
55. T. Su, P. C. Taylor, G. Ganguly and D. E. Carlson, Phys. Rev. Lett. **89**, 015502-1 (2002).
56. H. Fritzsche, Ann. Rev. Mat. Res. **31**, 47 (2001), and references therein.

57. S. Zukotynski, F. Gaspari, N. Kherani, T. Kosteski, K. Law, W. T. Shmayda and C. M. Tan, J. Non-Cryst. Solids **299**, 476 (2002).
58. P. Stradins and H. Fritzsche, J. Non-Cryst. Solids **200**, 432 (1996).
59. W. B. Jackson, D. K. Biegelsen, R. J. Nemanich and J. C. Knights, Appl. Phys. Lett. **42**, 105 (1982).
60. A. Yelon, H. Fritzsche and H. M. Branz, J. Non-Cryst. Solids **266-269**, 437 (2000).
61. T. Su, S. Chen, P. C. Taylor, R. S. Crandall and A. H. Mahan, Phys. Rev. **B62**, 12849 (2000).
62. J. A. Reimer, R. W. Vaughan and J. C. Knights, Phys. Rev. **B24**, 3360 (1981).
63. R. Biswas, Q. M. Li, B. C. Pan and Y. Yoon, Phys. Rev. **B57**, 2253 (1998).
64. S. Zafar and E. A. Schiff, Phys. Rev. Lett. **66**, 1493 (1991).
65. Q. Zhang, H. Takashima, J.-H. Zhou, M. Kumeda and T. Shimizu, Mat. Res. Soc. Proc. **336**, 269 (1994).
66. H. Dersch, J. Stuke and J. Beichler, Appl. Phys. Lett. **38**, 456 (1981).
67. N. A. Schultz and P. C. Taylor, Phys. Rev. **B65**, 235207-1 (2002).
68. D. L. Staebler and C.R. Wronski, Appl. Physics. Lett.**31**, 292 (1977).
69. J. Whitaker, J. Viner, P. C. Taylor, S. Zukotynski, N. P. Kherani, E. Johnson, and P. Strandins, Mat. Res. Soc. Proc. **808**,153 (2004)
70. S. Zafar and E. A. Schiff , Phys. Rev. Lett. **66, 1493** (1991).
71. P. Stradins and H. Fritzsche, Philosophical Magazine B **69**, 1 (1994)
72. N. A. Schultz and P. C. Taylor, Phys. Rev. B **65**, 235207 (2002)
73. R. A Street, Hydrogenated Amorphous Silicon (Cambridge Univ. Press, Cambridge, 1991)
74. H. M. Branz, Phys. Rev. B **59**, 5498 (1999)
75. M. Stutzmann, W. B. Jackson and C. C. Tsai, Phys. Rev. B **32**, 23 (1985)
76. J. A. Reimer, R. W. Vaughn, J. C. Knights, Phys. Rev. B **24** (1981)
77. P. Stradins, D. Young, Y, Yan, E. Iwaniczko, Y. Xu, R. Reedy, H. M. Branz, and Q. Wang; Appl. Phys. Lett. **89,** 121921, (2006).
78. D. L. Young, P. Stradins, Y. Xu, L. Gedvilas, R. Reedy, A. H. Mahan, H. M. Branz, Q. Wang, and D. L. Williamson, Appl. Phys. Lett, **89**, 161910 (2006).
79. M. M. de Lima, Jr, P. C. Taylor, S. Morrison, A. LeGeune, and F. C. Marques, Phys. Rev. B **65**, 235324-1 (2002). (And references therein)
80. M. H. Brodsky, R. S. Title, K. Weiser, and G. D. Pettit, Phys. Rev. B **1**, 2632 (1970).
81. J. Whitaker, J. Viner, S. Zukotynski, E. Johnson, P. C. Taylor, P. Stradins, *Tritium Induced Defects in Amorphous Silicon*, in *Amorphous and Nanocrystalline Silicon Science and Technology—2004*, edited by Gautam Ganguly, Michio Kondo, Eric A. Schiff, Reinhard Carius, and Rana Biswas (Mater. Res. Soc. Symp. Proc. **808**, Warrendale, PA, 2004), A2.3.
82. T. Ju, J. Whitacker, S. Zukotynski, N. Kherani, P. C. Taylor, P. Stradins (To be published).
83. For example see, J. H. Van Vleck, Phys. Rev. **74**, 1168 (1948); P. W. Anderson and P. R. Weiss, Rev. Mod. Phys. **25**, 269 (1953).
84. "*Elementary Electronic Structures"*, W. A. Harrison, (World Scientific Publishing Co. Singapore, Singapore, 2004).

REPORT DOCUMENTATION PAGE

Form Approved
OMB No. 0704-0188

PLEASE DO NOT RETURN YOUR FORM TO THE ABOVE ORGANIZATION.

1. REPORT DATE *(DD-MM-YYYY)*	2. REPORT TYPE	3. DATES COVERED *(From - To)*
September 2009	Subcontract report	1 February 2005 - 31 July 2008

4. TITLE AND SUBTITLE
Innovative Characterization of Amorphous and Thin-Film Silicon for Improved Module Performance: 1 February 2005 – 31 July 2008

5a. CONTRACT NUMBER
DE-AC36-08-GO28308

5b. GRANT NUMBER

5c. PROGRAM ELEMENT NUMBER

6. AUTHOR(S)
P.C. Taylor and G.A. Williams

5d. PROJECT NUMBER
NREL/SR-520-46649

5e. TASK NUMBER
PVB91110

5f. WORK UNIT NUMBER

7. PERFORMING ORGANIZATION NAME(S) AND ADDRESS(ES)
University of Utah
Salt Lake City, Utah

8. PERFORMING ORGANIZATION REPORT NUMBER
XXL-5-44205-09

9. SPONSORING/MONITORING AGENCY NAME(S) AND ADDRESS(ES)
National Renewable Energy Laboratory
1617 Cole Blvd.
Golden, CO 80401-3393

10. SPONSOR/MONITOR'S ACRONYM(S)
NREL

11. SPONSORING/MONITORING AGENCY REPORT NUMBER
NREL/SR-520-46649

12. DISTRIBUTION AVAILABILITY STATEMENT
National Technical Information Service
U.S. Department of Commerce
5285 Port Royal Road
Springfield, VA 22161

13. SUPPLEMENTARY NOTES
NREL Technical Monitor: Bolko von Roedern

14. ABSTRACT *(Maximum 200 Words)*
We performed collaborative research with United Solar Ovonics Corporation on defects that contribute to the Staebler-Wronski effect in modules made using a-Si:H and a-SixGe1-x:H intrinsic layers. Specifically, we performed electron spin resonance on a set of device-quality samples, half of which were light-soaked. We also performed nuclear magnetic resonance experiments on these samples to investigate hydrogen doublet sites. In addition, we investigated the defects generated in tritiated a-Si:H at both 300 and 77 K in collaboration with scientists at NREL. Finally, we performed studies of light-soaking at 77 K to compare the kinetics with those for the creation of defects at 77 K by tritium decay.

15. SUBJECT TERMS
PV; amorphous; thin film; silicon; module performance; innovative characterization; electronic spin resonance; nuclear magnetic; Satebler-Wronski effect;

16. SECURITY CLASSIFICATION OF:			17. LIMITATION OF ABSTRACT	18. NUMBER OF PAGES	19a. NAME OF RESPONSIBLE PERSON
a. REPORT	b. ABSTRACT	c. THIS PAGE			
Unclassified	Unclassified	Unclassified	UL		19b. TELEPHONE NUMBER (*Include area code)*

Standard Form 298 (Rev. 8/98)
Prescribed by ANSI Std. Z39.18